A HELIX TRACK FITTING PROGRAM

FOR

THE SILICON VERTEX TRACKER (SVT)

IN

THE SOLENOIDAL TRACKER AT RHIC (STAR) EXPERIMENT

by

JOSEPH WILLIAM BIELECKI

THESIS

Submitted to the Graduate School
of Wayne State University,
Detroit, Michigan

in partial fulfillment of the requirements
for the degree of

MASTER OF SCIENCE

1993

MAJOR: PHYSICS
Approved by:

Adviser date

To Almighty God

and then to my faithful wife, Ivonne

Acknowledgements

Through the development of this thesis many people have given support and encouragement. Most gratitude goes to my wife Ivonne, who has been very patient and selfless during our first three months of marriage, and my adviser Dr. Rene Bellwied, who has made this possible. I would like to thank everyone in the RHIC group at WSU for making the computer simulation laboratory, where most of the work was done, a friendly and productive environment, especially, Renato Matheus, who spent many hours with me to get LATEX to do just what I wanted and Gabe Roger, who helped me many times with FRITIOF and GEANT. Finally, I want to thank my immediate family and their hospitality to my wife and I, while I finished. Now, please, appreciate the work put forth.

Hebrews 11:1-3

Now faith is the substance of things hoped for, the evidence of things not seen. For by it the elders obtained a good report. Through faith we understand that the worlds were framed by the word of God, so that things which are seen were not made of things which do appear.

Contents

List of Tables

List of Figures

Chapter 1

Background

1.1 The Scientific Motivation for STAR

The purpose of the heavy ion Au-Au high energy relativistic collision experiment, the Solenoidal Tracker At RHIC (Relativistic Heavy-Ion Collider) (STAR), is primarily to detect signatures of quark-gluon plasma (QGP) formation and investigate the phenomena of strongly interacting matter at high energy density. The correlation of many observables on an event-by-event basis will be crucial. These correlations will be used to identify possible QGP signatures and special events. Thus, the detection system for STAR must be capable of measuring many experimental observables simultaneously. Even if signatures for the QGP are not explicitly determined, the detector system should be versatile enough for other special events. The motivation and goals of the STAR experiment will provide a foundation for the physics and purpose beyond the silicon vertex tracker detector and the data processing developed in this study which culminates in a thesis.

1.2 The Specific Goals of STAR

At RHIC, two fundamentally new aspects of hadron production will be implemented: correlations between global observables on an event-by-event basis and the use of hard scattering of partons as a probe of the properties of high density nuclear matter. Very high charged particle densities, $dn_{ch}/d\eta \approx 700$ expected in nucleus-nucleus collisions, provide a favorable environment for event-by-event measurement of global observables. The experiment will be designed to detect event-by-event fluctuations expected near phase transitions by monitoring threshold behavior of the experimental observables as a function of energy density. Full azimuthal coverage of particle identification and continuous tracking will provide maximum particle yields needed for successful measurements. Hard QCD processes can be investigated due to jet yields at RHIC. This can be reached by tracking combined with segmented electromagnetic calorimetry and high p_t single particle measurements. Possible QGP characteristics can be observed by measuring hadronic cascades of hard-scattered partons. This measurement will also give new information on the nucleon structure function and parton shadowing in nuclei. Inclusive and event-by-event observables for proton-proton, proton-nucleus, and nucleus-nucleus interactions are measurement requirements for the STAR experiment. To conclusively identify signatures of QGP formation all observables will be studied as a function of impact parameter and incident energy [1].

1.3 Definition of Terms

1.3.1 Global Observables

The term global observable is used for variables or parameters which are defined to represent the collision dynamics for an event in an experiment in general terms [2]. By example, it will become more clear. A useful variable for locating the scattered particles after the collision is rapidity defined as

$$y = \frac{1}{2} ln \left(\frac{E + p_z}{E - p_z} \right), \tag{1.1}$$

where E is the energy of the particle and p_z is the momentum in the z or beam axis. Because the energy is high, the particles created are approximately relativistic and the rapidity parameter which is Lorentz invariant is well suited for describing particle positions and energy distribution. A more convenient variable related to the rapidity, but which does not require knowing E or p_z, is called pseudo-rapidity.

$$\eta = \frac{1}{2} ln \left(\frac{1 + cos\theta}{1 - cos\theta} \right) = -ln \left(tan\frac{\theta}{2} \right) \tag{1.2}$$

Pseudo-rapidity requires only the polar angle θ between the momentum direction of the scattered particle and the beam axis. For very high transverse momentum ($p_t \gg m$, the rest mass), pseudo-rapidity and rapidity are approximately equal ($y \approx \eta$). At this energy, no particle identification is needed to determine the rapidity.

One other variable of interest is the total transverse energy, which describes the transfer of incident energy from the colliding baryons to created mesons, mostly pions.

This energy is defined as

$$E_t = \sum_i E_i sin\theta_i, \tag{1.3}$$

where i sums over all the particles and θ_i is the angle between the momentum of the particle i and the beam axis. This variable (E_t) can be measured directly and is closely related to the energy density of the collision [3].

1.3.2 Parameters for Particles Traversing Matter

At high energies, it is convenient to measure the thickness of a material by a more common scale than that of a meter stick. Therefore, the mean distance for the energy of a high-energy electron to be reduced to $1/e$ by bremsstrahlung, is defined as the radiation length X_o for that particular material. Y. S. Tai has calculated and tabulated X_o [4], and an approximation can be made with the following analytical function:

$$X_o = \frac{716.4\ g\ cm^{-2} A}{Z(Z+1)ln(287/\sqrt{Z})}, \tag{1.4}$$

where Z and A are the charge and the mass number of the medium [5].

When a charged particle passes through a medium many small-angle scatters occur and in most cases these deflections are a result of Coulomb scattering from nuclei. The name given to this phenomena is multiple Coulomb scattering (MCS). (Note that hadronic projectiles have a strong interaction which contributes to multiple scattering.) The theory of Molière simulates the Coulomb scattering distribution closely. The distribution is Gaussian like for small angles of deflection, but has a broader base at large angles taking on a Rutherford scattering behavior.

By defining

$$\theta_o = \theta_{plane}^{rms} = \theta_{space}^{rms}, \tag{1.5}$$

this accounts for the most central 98% of the projected angular distribution in the Gaussian approximation which is acceptable for many applications. The width of the distribution is then found by

$$\theta_o = \frac{(13.6\ MeV)z}{\beta cp}\sqrt{(x/X_o)}(1 + 0.038ln(x/X_o)), \tag{1.6}$$

where p is momentum, βc is velocity, z is the charge number of the incident particle, and x/X_o is the thickness of the medium scattered through in radiation lengths [6].

1.3.3 Definition of χ^2: Goodness of Fit

When the process of representing physical data through a function is attempted, a parameter is defined to establish criteria for optimizing the fit. χ^2 is that value and is defined as

$$\chi^2 \equiv \sum_i \left(\frac{(y_i - y(x_i))^2}{\sigma_i^2}\right). \tag{1.7}$$

Where y_i is a dependent variable representing experimental data, $y(x_i)$ is the calculated value for y as a function of the independent variable x_i, and σ_i is the expected spread or resolution of the measurement. The concept is derived from the method of least squares for curve fitting by assuming the method of maximum likelihood which says the observed set of measurements is more likely to have come from the actual parent distribution than from any other, while assuming a Gaussian distribution with σ_i as the standard deviation for the experimental observations about the actual value. The probability for any x_i to measure y_i is

$$P_i = \frac{1}{\sigma_i\sqrt{2\pi}} exp\left(-\frac{1}{2}\left(\frac{y_i - y(x_i)}{\sigma_i}\right)^2\right). \tag{1.8}$$

The probability of making a set N of measurements y_i is the product of these probabilities.

$$\prod_i P_i = \prod_i \frac{1}{\sigma_i\sqrt{2\pi}} exp\left(-\frac{1}{2}\sum_i\left(\frac{y_i - y(x_i)}{\sigma_i}\right)^2\right) \tag{1.9}$$

From the equation above, it can be seen that to maximize the probability the negative exponent, which is just $\chi^2/2$, is to be reduced [7].

Chapter 2

Overview of Experiment

2.1 Design Concept and Criteria

A large acceptance device with simultaneous measuring capacity for both soft and hard physics is desired. The design criteria for soft physics are:

- detection of as many charged particles as possible with high efficiency, to provide high statistics for event-by-event observables and fluctuation studies
- 2π continuous azimuthal coverage for reliable event characterization
- high tracking efficiency as close to the vertex as possible, to contain the size and cost of the experiment
- adequate track length for tracking, momentum measurement and particle identification for a majority of the particles
- high kaon detection efficiency for event-by-event observables and for inclusive measurement of the ϕ-meson
- momentum resolution $\Delta p/p \leq 0.02$ for $p_t < 1.5$ GeV/c
- two-track resolution providing a momentum difference resolution of a few MeV/c for HBT correlation studies.
- accurate determination of the primary vertex for high momentum resolution and to be able to identify particles from the primary interaction
- accurate determination of secondary vertices for detecting strange particle decays such as $\Lambda, \bar{\Lambda}$, K_s^o, Ξ^+, Ξ^-, and Ω^-

The objectives for the hard physics phenomena, which the SVT will have less of a role in determining, are:

- large uniform acceptance to maximize rates and minimize edge effects in jet reconstruction
- accurate determination of the primary vertex in order to achieve a momentum resolution $\Delta p/p < 0.05$ for $p_t = 10$ GeV/c for high p_t particle spectra and jets
- electromagnetic calorimetry combined with tracking and good momentum resolution up to $p_t = 10$ GeV/c to measure and trigger on high E_t jets
- 2π azimuthal coverage of electromagnetic calorimetry for event characterization
- linear response of electromagnetic calorimetry for accurate energy measurements
- segmentation of electromagnetic calorimeters which is an order of magnitude finer than the typical jet size, i.e. jet radius $r = \sqrt{d\eta^2 + d\phi^2} \sim 1$

The design of the detection system of the experiment is conformed to the physics goals. Most of the midrapidity charged particles, including their tracking, momentum analysis, and particle identification, need to be detected. Track detection must be obtained in higher than expected maximum charged particle multiplicities for central collisions ($n_{ch} = 3000$ in the range $|\eta| < 1$ at midrapidity). Pions/kaons can be distinguished for $p < 0.7$ GeV/c and kaons/protons can be distinguished for $p < 1$ GeV/c via dE/dx. Decay particles will be measured and their second vertices will be reconstructed. Resolution at a 2 m radius from the vertex is expected to be 2 cm. Momentum resolutions ($\Delta p/p$) of 0.02 at 0.1 GeV/c are needed for conformation of the physics expected, and $\Delta p/p$ in the order of a few percent is necessary for $p = 10$ GeV/c to measure rapidly falling spectra at high p_t and particles from jets. Limiting momentum resolution at low p_t is due to multiple scattering, which will be minimized by keeping detector material minimal through all of the detection system. Figure 2.1 shows the STAR experiment detectors.

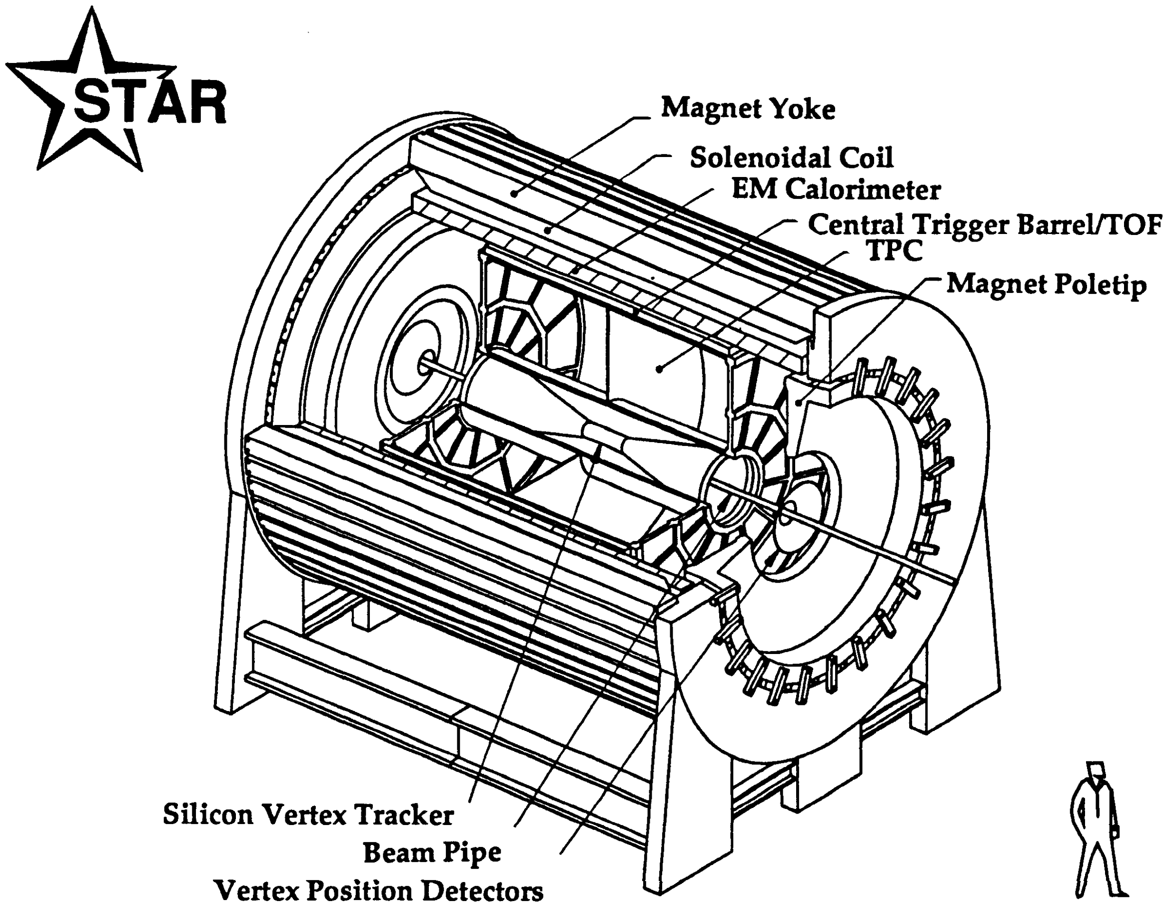

Figure 2.1: *The STAR detector geometry setup.*

For a large pseudo-rapidity range ($|\eta| < 2$) at midrapidity with complete azimuthal coverage ($\Delta\phi = 2\pi$), momentum will be measured. In the range $|\eta| < 1$, particle identification will be obtained. The information that the detection system will provide is tracking and momentum analysis through a time projection chamber (TPC) and silicon vertex tracker (SVT) encompassed by a solenoidal magnet, particle identification via dE/dx, and position of primary and secondary vertices. A collision geometry trigger will be provided by the following specific detector components:

- a central trigger scintillator barrel around the TPC
- vertex position detectors near the beam line but outside the magnet.
- calorimeters located in the area of the beam insertion magnets to reject events dictated by the number of spectators

Furthermore, the electromagnetic calorimeter might reside inside the solenoidal magnet for triggering on transverse energy and jet cross sections.

Various characteristics and topologies of events and collision geometry will be available through a number of triggering detectors. The tracking of the percentage of particles with charge will range to $|\eta| < 2$. Track information will be accessed from the silicon vertex tracker (SVT), which will be able to fit primary vertex tracks and determine secondary vertex tracks of decaying particles below a 6 cm radius constrained by the geometry of the detector, and a time projection chamber (TPC) inside a solenoidal magnet producing a helical path for continuous tracking, accurate momentum resolution and particle identification. It should be noted that the SVT will provide useful track information to a range of $|\eta| < 1$.

The physics of the STAR Experiment demand acquiring information of projectiles from protons to Au, available beam energies, and impact parameters. From minimum bias to centralized collision geometry trigger range, soft physics processes will be studied, and later on more refined methods of triggering will be one of the essential points of ongoing STAR. Rare events and jet production studies are believed to be obtained through longer data acquisition periods [1].

2.2 Magnetic Field

The solenoidal magnet around the TPC and SVT will produce a uniform field along the beam direction. Field strength will be a maximum of 0.5 T. Shaping the magnetic field will be done through an iron return yoke and shaped pole pieces. This design is to facilitate high tracking accuracy and azimuthal symmetry. Other smaller coils will be used to enhance uniformity of the field. The strength maximum was chosen to allow resolution of tracking particles with momentum as high as 10 GeV/c. Low p_t particles will also have reasonable tracks.

2.3 Time Projection Chamber (TPC)

The TPC will have two longitudinal drift sections, each 2.1 m long. The particle carriers created from the ionization will drift in the longitudinal direction, due to the electric field in the TPC, to its end-caps. 70,000 pads make up each end-cap. Two pad sizes, one for 50 cm$<$radius$<$125 cm (2.85 mm x 11.5 mm) and one for 125 cm$\leq$radius$<$200 cm (6.2 mm x 19.5 mm) will be implemented. The pads will readout into 512 time samples. Ignoring energy losses, singly-charged particles with $p_t <$ 40 MeV/c will spiral inside the inner radius of 50 cm of the TPC. Only those singly-charged particles with $p_t >$ 150 MeV/c will spiral completely through to the outside radius of 200 cm of the TPC. The acceptance hence is limited to the longitudinal length and inner and outer radius of the TPC, giving a value of $|\eta| < 1$ for outer radius and $|\eta| < 2$ for all particles which reach the inner radius, but not necessarily traverse completely through to the outer.

2.4 Silicon Vertex Tracker (SVT)

The purpose of the SVT is to extend the resolution of the TPC closer to the vertex to position primary interaction vertices, improve momentum and dE/dx resolutions, and determine secondary vertices to an accuracy less than 100 μm. Positioned closer to the vertex collision, the SVT will extend the acceptance of the TPC for momenta lower than 150 MeV/c. The SVT will provide this information by storing three dimensional space points and resulting tracking vectors with high resolution. From this track information, the SVT can be linked to the TPC to continue tracking of projectiles. Low mass material for the SVT is essential to avoid high secondary particle production, photon conversion and high multiple scattering.

The SVT will consist of 216 silicon drift detectors (SDD) overlapped by a percentage due to dead detector area. Other designs for the SDD's are still being considered depending upon important parameters such as efficiency, cost, manufacture, etc. The wafers are attached in a line of 4, 6, and 7 respectively, designated as ladders. The ladders are connected in the shape of polygon barrels of 8, 12, and 16 to encompass the colliding beams and their point of interaction. The thickness of each individual wafer is 300 μm which produces 24,000 electrons for a minimum ionizing particle. This is an acceptable signal strength taking into account multiple scattering and secondary particle production. The front end electronics is laid out to characterize up to 50 times minimum ionizing particles (e.g. very low momentum protons, p $\approx$ 100 MeV/c).

2.4.1 Specific SVT Detector Description

The SVT is based on the need of high spacial resolution for the tracking of charged particles very close to the primary vertex. Placed inside the TPC, it measures around 30 cm. in diameter at its outer layers of polygon shaped barrels made of ladders of silicon wafers positioned to achieve highest efficiency of tracks detected. Presented in figure 2.2 and in table 2.1 is the latest version for the proposed SVT geometry and its specifications. Notice, the relatively new design of double layering of each polygon barrel and end regions for electronic data acquisition. It's future specific shape and size, like the SDD, depends upon the interface of many factors still pending: cost, design of silicon wafers, configuration for best efficiency, etc.

For developing a fitting program for spiraling tracks produced by charged particles in a 0.5 Tesla magnetic field near the vertex of the collision, only four space points, one being the vertex, on or near a helix path are collected and needed at relative positions from the vertex. The three remaining space points (hits in the detector) are collected in SDD's classified as semiconductor memory detectors. This type of detector works on the same principle as of the classical semiconductor detector, but when charges are produced within the drift detector by ionizing particles, they are not removed and detected immediately. The charged carriers (usually electrons) are stored in the volume of the detector and then, transported in a controlled way parallel to the surface of the detector to a readout electrode with the position information intact. The migration of these carriers occur due to the setup of an electric field in the material, hence the carriers, if electrons, will fall towards the least negative potential where they rest until transferred out and processed by a preamplifier. The positions

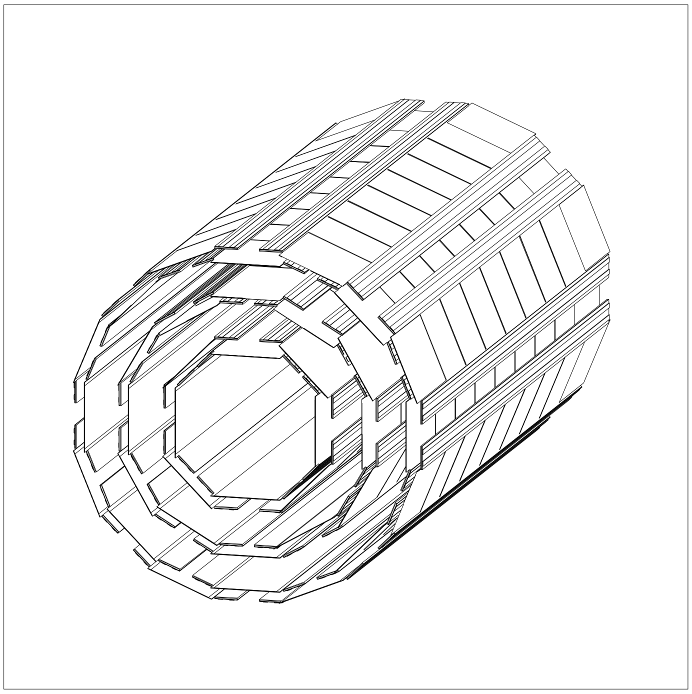

Figure 2.2: *The Silicon Vertex Tracker with recent design developments.*

Table 2.1: *Some specifications of the developing Silicon Vertex Tracker for STAR.*

Silicon Vertex Tracker	
length (active area)	42 cm (max.)
Inner Barrel (radial distance)	5.97 cm
Middle Barrel (radial distance)	10.16 cm
Outer Barrel (radial distance)	14.91 cm
Thickness of wafer (SDD)	300 μm
Total Thickness	900 μm $\sim$ 0.9% X_o
Number of wafers	216
Inner Barrel	32 (8$\times$4)
Middle Barrel	72 (12$\times$6)
Outer Barrel	112 (16$\times$7)
Diameter of wafer (SDD)	10.16 cm = 4 in
Length of wafer (SDD)	6 cm
Width of wafer (SDD)	6 cm
Drift Length of wafer	3 cm
Average Drift Time	3 μs
Time Samples	256
Sampling Rate	40 MHz
Anode Pitch	250 μm
Number of Channels	103680
Position Resolution	$<$ 25 μm

the carriers are stored in before the information is read out are elementary memory units (pixels) engineered in such a way that the carriers are restrained to that unit region, not able to leap into others. At some later time, with the corrected sequence and amount of voltages applied to the electrode configuration, the carriers confined to the corresponding pixels are shifted out one pixel after another with no loss of particle carriers [8].

2.5 Electromagnetic Calorimeter (EMC)

The EMC will measure and trigger on the total E_t and local $d^2E_t/d\eta d\phi$ transverse energy deposition in p-p, p-A, and A-A collisions. From the soft nuclear processes, the temperature and energy density of the reaction can be determined by analyzing the transverse energy at mid-rapidity. Triggering on jets, high energy direct photons, and high p_t particles can be accomplished with the EMC. Properties of interactions of hard scattered partons in the hot nuclear medium may be inferred from this information. Spin structure of polarized pp collisions can be investigated as well as single spin transverse asymmetries. The barrel of the EMC is made of lead-scintillator located inside the superconducting solenoid coil and inside the iron flux return. Its coverage is $|\eta| \leq 1.05$ and 2π in azimuth. Energy resolution for the EM calorimeter is expected to be near $0.20/\sqrt{E}$.

2.6 Triggering and Trigger Detectors

A particular signature for the quark-gluon plasma is not known yet, so the triggering must be versatile in that it is able to explore various paths and flexible to upgrades and adoption when understanding grows. High dead times will be used in the start of STAR until enough information is collected to selectively trigger. The goals of the triggering detectors are:

- detect Au-Au interactions with $>$ 95% efficiency
- detect p-p interactions with $>$ 50% efficiency
- locate Au-Au vertex to within ± 6 cm within < 200 ns
- detect multiple events occurring within 40 μs with 90% efficiency
- select highest 2.5% of multiplicity or E_t distribution in < 200 ns
- select high transverse electromagnetic energy
- select based on geometry of hit patterns
- allow simple integration of upgrades to trigger system

The interaction rates for Au-Au and p-p are expected to be 1 kHz and 1 MHz with the event recording rate expected to be 1 Hz and 30 Hz, respectively. The trigger system will prioritize the events and select those of higher priority from the sample of events. Events can be selected out during the TPC readout/digitization, but not during the drift time-window.

The scale for trigger decision time is based on three natural time scales for STAR:

1. the crossing time of 110 ns
2. the maximum drift time in the TPC of 40 μs
3. the readout/digitization time for the TPC of 10 ms

Within these ranges of time (0 to 110 ns; 110 ns to 40 μs; 40 μs to 10 ms), the trigger is a process. The first level is based on vertex location and centrality, the second on the geometry of hits, and the third on software decisions of tracking information. Each process of the trigger decision time is expected to have keep/flush decision capability. The detectors of the trigger system and their acceptance ranges are in table 2.2.

Table 2.2: *The detectors contributing to the trigger process. Note, ϕ from 0 to 2π.*

Detector	$\|\eta\|$	*# of Channels*
Central Trigger Barrel (CTB)	0 - 1	200
TPC Endcaps (MWPC)	1 - 2	2000
Vertex Position Detectors (VPD)	3.3 - 3.8	50
Veto Calorimeter (VC)	> 5	2
EM Calorimeter (EMC)	0 - 1	1200

2.7 Data Acquisition (DAQ)

The newest transputer family members, the T9000 RISC processor and the C014 pacet router, will be the base of the DAQ process and chosen because of cost, hardware, and software. The DAQ subsystem will have a twofold function in the experiment. One function is an event builder, by assembling data originating from the detector subsystem into an acceptable form for recording and distribution through an analysis network. The other task is high level triggering based on event building and third-level triggers. Data recording rates are limited to the speed of tape recording, but inputs to the trigger processors will be > 50 events/sec. To store a single central Au-Au collision event, the expected allocated data rate is 96 MB, but after zero suppression this can be reduced to 16 MB (14 MB for TPC; 1 MB for SVT; 1 MB for all other systems). These events are to be recorded on magnetic tape at the rate of 1 event/sec. At the rate of 30 event/sec, p-p collisions will be stored, which are much lower in multiplicity than Au-Au collisions. It is expected that online data analysis (data reduction and compression due to track determining and fitting) will increase the recording rate [1].

Chapter 3

Physics of the SVT for STAR

3.1 Physics of STAR

There are two objectives to be accomplished in the STAR Experiment:

1. the investigation of soft physics processes like hadron production at transverse momenta below 1-2 GeV/c
2. the study of hard QCD processes, specifically jet, mini-jet, and hard photon production

The essential measurements in STAR to detect QGP signs will consist of

1. proton-proton, proton-nucleus and nucleus-nucleus interactions
2. impact parameter dependence
3. dependence on incident energy

The soft physics aspect of the objectives will be met by the inclusion of the SVT which will extend the acceptance of the TPC to low p_t. The list of particles aimed to observe directly are π^+, π^-, K^+, $K^-, p, \bar{p}, d$, and $\bar{d}$. Particles like $K_s^o, \phi, \Lambda, \bar{\Lambda}, \Xi^-$, and Ω^- will be implicitly detected through their charged particle decay schemes. Rare decays, like the open charm or strange composite objects, might be accessible with the SVT, which are discussed in the text as QGP signatures. The following chapter will emphasize the physics goals relevant to the SVT and leave other issues for the reader to find in the CDR of STAR or in related publications [1].

3.2 Physics Related to the SVT

3.2.1 Low p_t Phenomena

The phenomena related to pion p_t-spectra under 200 MeV/c is not understood completely for RHIC interactions [9] [10] [11] [12], so with the extension to low momenta with the high resolution of the SVT the information collected on particle species like kaons, pions, and protons could provide the foundation of a better description.

Collective effects can generally be applied to the correlations of low p_t particles. 'Van Hove bubbles' [13], localized plasma formation, might lead to correlated hadronization of low p_t particles and this can be verified by measuring fluctuations of the yield in rapidity. Information on the yield of low p_t charged pions on an event-by-event basis, as well as their correlation behavior as a function of centrality may lead to some information about the hadronization of a chiral condensate which would give support to the theory that in the cold phase different orientations in a vacuum are present in as opposed to outside of a QGP bag [14]. In combination with the EMC, isospin fluctuations in the π yield could be measured on an event by event basis by investigating the $\pi^{\pm}/\pi^{o}$ ratio. Unusual ratios were found in cosmic ray measurements (centauro event). Several different theories like Bose-Einstein condensation [15] or disorientation of the chiral condensate [16] are proposed.

3.2.2 Flavor Composition

Characteristics of the collision such as thermalization, expansion, and hadronization will be determined by the yield and spectral distribution of particles composed of heavy quarks. A signature for the formation of the QGP may be revealed through this measurement of abundances and spectra. In particular the ratio of strange to anti-strange baryons is proposed as a signature. These ratios should reveal a systematic trend as a function of increasing strangeness (Λ, Ξ, Ω) which is due to net zero strangeness, a property of a QGP phase [17].

In general, strange particle detection is one of the primary goals of STAR. One aspect that the SVT can provide some incite to is observables dependent on increased strangeness density produced by the presence of multi-strange baryons (e.g. Ξ^-, Ω^-, etc.) which if present will decay with short decay-lengths of $c\tau \approx$ 1-10 cm. The SVT should be capable of tracking these secondaries that decay within the first layer and such speciation of particles identified could provide evidence for a QGP signature. The SVT will uniquely provide information on asymmetric decays (One branch of the decay has $p_t <$ 300 MeV/c). A high resolution mass reconstruction is of particular interest for the ϕ meson. A modification in the width of the ϕ meson peak can be measured by STAR via its K^+K^- decay channel. The superior momentum resolution of the SVT-TPC combination allows a peak width determination down to the MeV level. The clarification in peak width due to medium modifications ('dropping mass model') is proposed as a QGP signature [18] [19]. This requires accurate position resolution of the SVT as close to the beam pipe as possible to distinguish primary tracks from secondaries. Longer decay-length strange particles like kaons and pions will be identified by energy loss through both the TPC and SVT.

For charmed particles (e.g. D^o and $D^{\pm}$) the situation is less convenient, because their production cross sections (σ_c/σ_s) and life times ($c\tau \approx 200\ \mu$m) are small. Although, with the contribution of the SVT to increase the resolution near the primary interaction charmed particle production may be observed. For example, $D^o(\bar{D^o})$ decaying into K$^-$ + π^+ (K$^+$ + π^-) 3.7% of the time is a trackable secondary scheme for the SVT.

A first scheme, relying on the back reconstruction of the complete D meson-decay chain for an invariant mass reconstruction was tried at Warsaw University. This analysis would lead to a full characterization of the D-production by measuring the yield and the kinematic properties (4-momentumvector) of the D meson. Preliminary results show a marginal chance for separating the D from the random background, constituted by the charged particle emission in a Au-Au event.

An alternative route, relying on measuring one specific decay particle (in this case the K, $D\ \rightarrow$ K+anything (22%)) is studied at Wayne State University. Continuation of the kaon vertex spectrum in a window close to the primary vertex (impact parameter b = .5 to 1 mm) can only arise from the tail of the primary vertex distribution due to multiple Coulomb scattering. No other particle decay provides this signature. Only the abundance of D mesons can be probed with this method. No kinematic information is obtainable. The yield of $D's$ is proposed as a definite signature for QGP by several authors [20]. First results of the simulation are encouraging and are detailed in a STAR note [21].

Chapter 4

Algorithms for the SVT Data Processing

4.1 Introduction to the Hardware and Software

To run the simulation of a complete STAR event a Silicon Graphics Workstation was employed utilizing the GEANT software package for geometry and tracking [22], and the FRITIOF (LUND Monte Carlo) for event generation [23][24]. For a detailed description of the LUND software see [25]. The software initiates a geometry program written to interface with GEANT through its corresponding subroutines. Figures 4.1 and 4.2 show the simplified geometry design and tree used for the study.

Actually, the design is more complex with the ladders made of wafers, with fixtures, and overlap. Having ignored the fixtures and the overlap, creates less deviation from helical tracks which increases efficiency, because some tracks will track through this material as well as the active regions of interest experiencing enhanced MCS. This developed software for processing the data is independent of the input track array and its geometry and tracking process, so a more realistic geometry and tracking can be implemented.

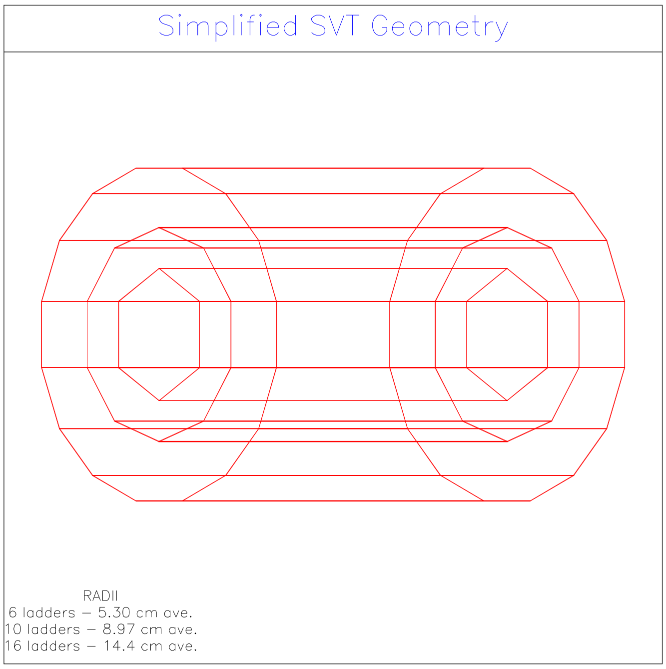

Figure 4.1: *SVT simplified geometry.*

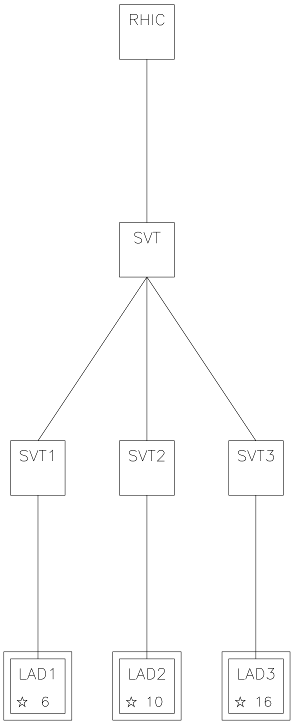

Figure 4.2: *The tree chart of the geometry of the SVT.*

In addition to this geometry of sensitive and active wafer volumes, Au-Au collisions at 200 GeV/u in a collider mode are produced by FRITIOF and tracked through the detector geometry using GEANT software. As the tracks traverse the active regions space points (hits) are stored in a data file. This file of three-dimensional space points stored in an array is sent to the cone procedure where all possible tracks of three points, each from a different layer within the cone dimensions, are collected. This expanded array is sent to the helix fit where tracks with the lowest χ^2 are stored in a final fit array carried on to an efficiency routine. The following flow chart in figure 4.3 displays the order and path of the routines.

4.2 Cone Restriction (SVT FILL & SVT FILL SEC)

SVT FILL does the cone development over all three layers of the SVT. Input is a space point array from GEANT tracking. The cone procedure consists mainly of three nested DO loops. The first loop stores the space points of the first layer and projects a cone on the second layer. The second loop stores along with the corresponding first layer point any selected space points on the second layer that fall within the limits of the cone. The same format applies for the third layer projected from the second. The dimension of the third layer cone is twice that for the second. The cone dimension is comprised of MCS angle as the particle traverses the silicon layers (which is a function of radiation length as shown in equation 1.6), the bending due to the magnetic field, and the resolution of the space points and vertex. Therefore, the resulting output contains all possible combinations of space points that construct a track within the

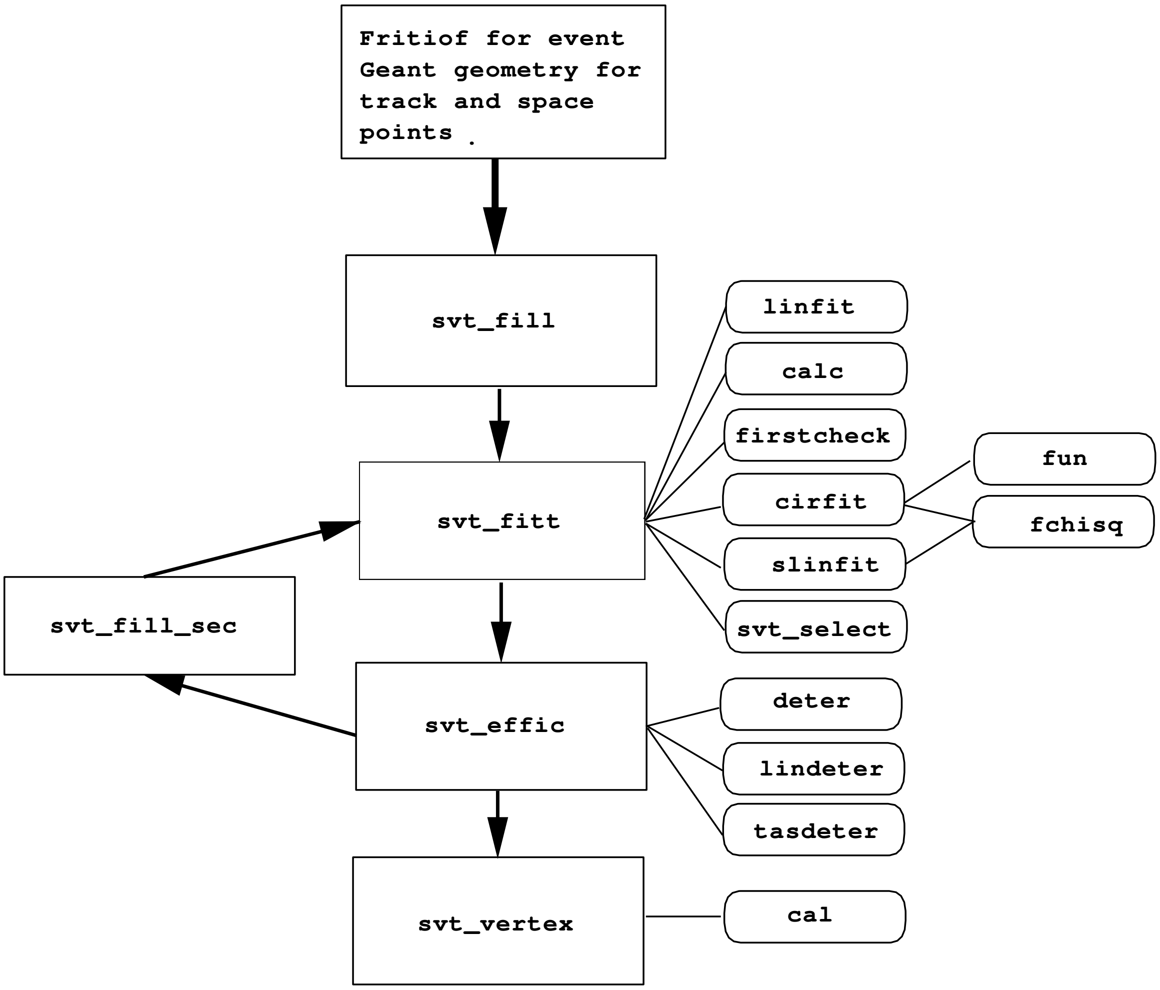

Figure 4.3: *The flowchart of the system of subroutines to fit SVT space points to helical tracks.*

predetermined cones. The arrays then input to the helix fit subroutine.

The projection of the cone from layer to layer is composed of two approximations. First, the space point's x, y, and z components, of the first layer are multiplied by the ratio of the average distance from vertex to the second layer (R_{ave2l}) to the average distance to the first layer (R_{ave1l}) to obtain a projected second layer space point (x_{proj2}). Explicitly,

$$x_{proj2} = x_1 \left(\frac{R_{ave2l}}{R_{ave1l}} \right). \tag{4.1}$$

This calculation assumes linearity in the x, y, and z directions. The second calculation is to add and subtract a determined deviation on the projected x, y, and z values to produce an area (in the xy plane) or a volume (in 3 dimensions) which is called a cone region. This region is then used in the condition to simulate a real data event giving the algorithm a choice of original and ghost tracks by selecting all space points in this cone. The same procedure is performed from the second to the third layer except that the deviation is doubled.

The deviation in projecting to the next layer can be quantified by taking into account bending of the track by the magnetic field, the variance from helical tracks due to MCS, and an assumed position resolution with a vertex resolution which produces a deviation in all directions taking the thickness of silicon detector traversed and the distance between the first and third layer into account. Where as the position and vertex resolution are constant, the bending due to the magnetic field and the MCS are dependent upon the transverse momentum of the particle (see figure 4.4 and 4.5). A fixed cone that accounts for these deviations can be determined but, as seen in figure 4.7, the gathering of ghost tracks increases rapidly for larger cones. For example, from figure 4.5, at 0.1 GeV/c the projected deviation of a proton from MCS is around 3.5 mm in absolute cone dimension. From figure 4.4, the projected deviation from the magnetic field is around 4.0 mm. The resolution of the vertex and space points combined is about 0.5 mm. From the plot of figure 4.7, this cone corresponds to a construction of about 12 tracks for every GEANT track. Figure 4.6 shows the cone efficiency is near 80% for an absolute cone dimension of 8 mm. Cone efficiency is defined as the number of original tracks reconstructed to the total number of original tracks. It is clear from the curve that a cone efficiency of at least 95% dictates a

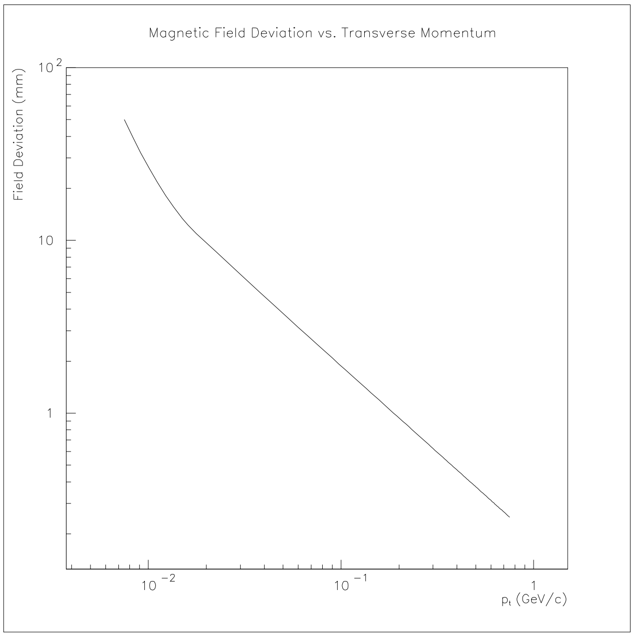

Figure 4.4: *The deviation of the track of a charged particle from a straight line due to the magnetic field at the first layer as it depends upon the transverse momentum of the particle.*

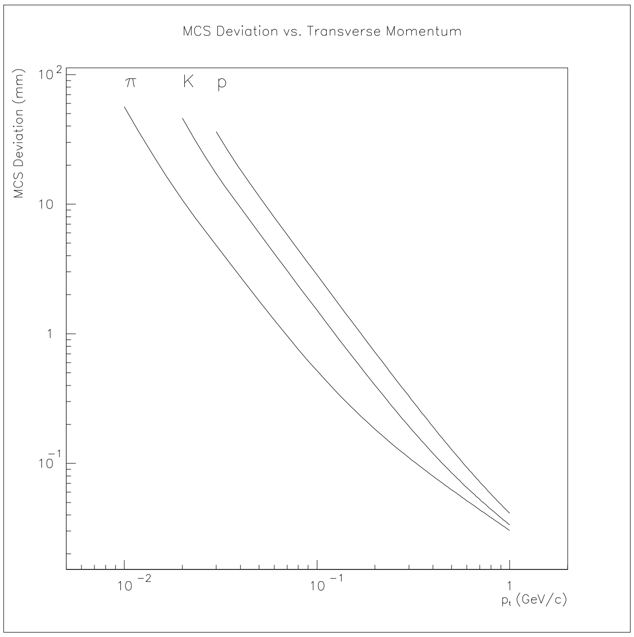

Figure 4.5: *The deviation of the track of a particle at the second layer due to MCS of the first layer as it depends upon the transverse momentum of the particle.*

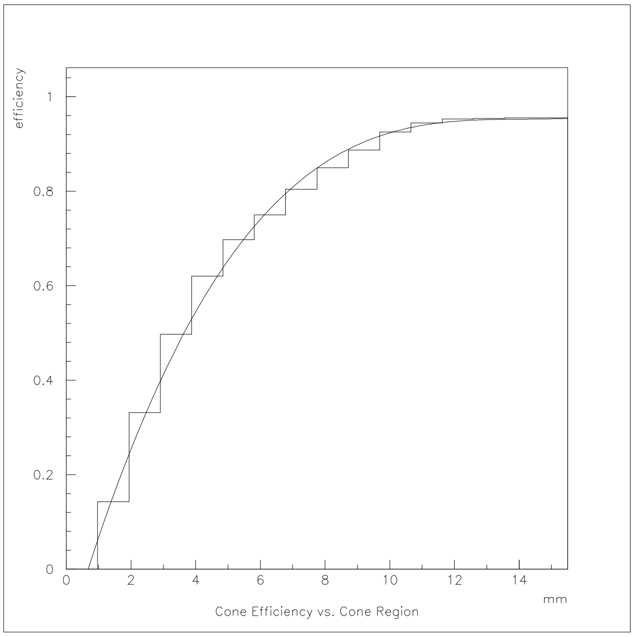

Figure 4.6: *The cone efficiency, as defined in the text, as it depends upon a fixed projected reconstruction cone in SVT FILL.*

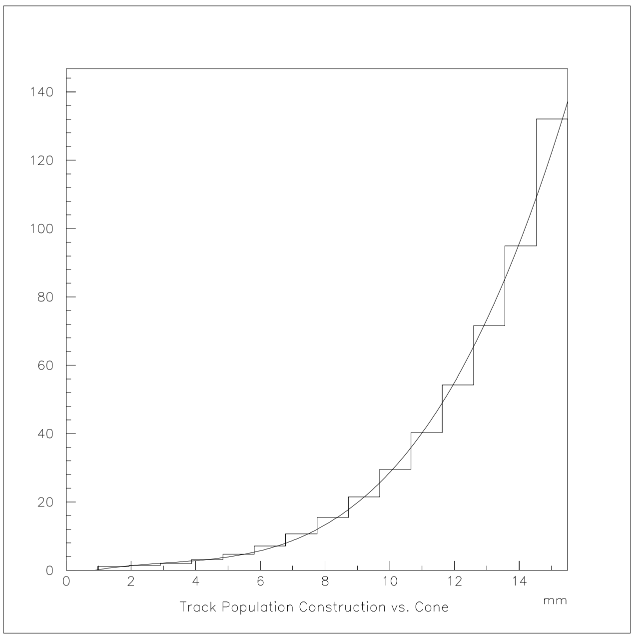

Figure 4.7: *The population of tracks constructed as a function of the fixed cone dimension in SVT FILL.*

fixed cone > 10 mm in absolute dimension (or 20 mm^2 in area). If the cone could be increased further, 100% of the original tracks would eventually be retrieved. Note from figure 4.7 that the number density of tracks assembled assuming an absolute cone projection dimension of 10 mm for one first layer space point is near 25. As a result of increasing the cone, the program will be slowed down due to the increased constructed ghost tracks along with the original tracks and a trade off must be made at some point to limit lag time of the fit procedure.

The cone can be fixed to a relatively large dimension for a complete event, but the fit efficiency will suffer as a result of the increased population of ghost tracks as will be shown in chapter 5. An alternative method is to iterate the fit procedure and increment the cone each time taking out those tracks found in that size cone. This reduces the number of ghost tracks significantly (see figure 4.8) and there will be an improvement in the total efficiency of the fit, since less ghosts tracks will be passed on to the fitting routine. Shown in figure 4.8 by iterating the cone, at the 10 mm cone dimension, the track construction density is about three and is actually decreasing for larger cone regions. For the example event, the cone increment is 1 mm, but the improvement can be enhanced even more by incrementing at smaller steps, eventually being optimized near the detector's resolution. If desired, 100% of original tracks can be coned before moving on to the fit by incrementing the cone out to the maximum track deviation from one layer to another with far less ghost tracks present in the array.

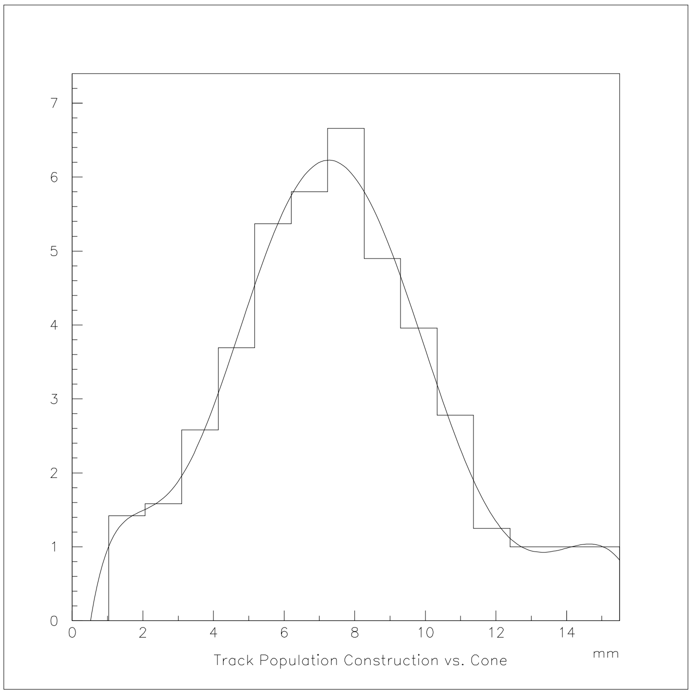

Figure 4.8: *The reconstruction track population as a function of an incremented cone as described in the text.*

4.3 Helix Fitting Algorithm (SVT FIT)

The method used to fit a helix to four space points first breaks the three dimensional curve into two separate two dimensional plots(see [26] for similar techniques). The xy plane is perpendicular to the beam axis so that the helical tracks appear as circular. The other plane for fitting is the sz plane which describes the motion of the helix in the z or beam direction. The program, written in FORTRAN, is an arrangement of subroutines for processing and fitting of SVT data points. The subroutines are:

- LINFIT - a least-square linear fit approximation
- CALC - the calculation of initial parameters for the helix
- FIRSTCHECK - a check to see if the track deviates far from a helix

- CIRFIT - a circle fit in the xy plane
- SLINFIT - a linear fit in the sz plane
- SVT SELECT - the selection of the lowest χ^2 tracks of each first space point

The function of these subroutines and other function subprograms used by the routines will be explained in the following pages.

The main part of the program consists of modules that receive an input of four space points to be fitted to a helix curve, and return fitted space point parameters and χ^2 of the track. After the four points are received, the track is checked to make sure the path progresses through each layer by comparing the absolute distance of each space point to each corresponding average silicon layer distance with some maximum and minimum limit. At this point, the first subroutine LINFIT is used to see whether the track can be approximated as a line in three dimensional space. The subroutine uses the sum of the deviations from the original data to the spatial resolution to determine the acceptability of the approximation. If the deviation sum is within the limit, the four space points are fit to a line using least-squares fit for a linear function.

$$y(x) = a + bx, \tag{4.2}$$

and the coefficients are determined by

$$a = \frac{1}{\Delta}\left(\sum \frac{x_i^2}{\sigma_i^2} \sum \frac{y_i}{\sigma_i^2} - \sum \frac{x_i}{\sigma_i^2} \sum \frac{x_i y_i}{\sigma_i^2}\right) \tag{4.3}$$

$$b = \frac{1}{\Delta}\left(\sum \frac{1}{\sigma_i^2} \sum \frac{x_i y_i}{\sigma_i^2} - \sum \frac{x_i}{\sigma_i^2} \sum \frac{y_i}{\sigma_i^2}\right) \tag{4.4}$$

$$\Delta = \sum \frac{1}{\sigma_i^2} \sum \frac{x_i^2}{\sigma_i^2} - \left(\sum \frac{x_i}{\sigma_i^2} \right)^2 [7]. \tag{4.5}$$

If the linear fit is not applicable, then the fit procedure moves on to the first calculation of the parameters in CALC of the helix equation in the xy plane, namely, the center x and y coordinates (A_1 and A_2) and the radius (A_3) of the circle. Ignoring the third dimension for now, the calculation knowing three space points ((x_1,y_1);(x_2,y_2); (x_3,y_3)) on a circle is just the analytical solution to three circle equations and three unknowns(A_1;A_2;A_3). Specificly,

$$A_3^2 = (x_1 - A_1)^2 + (y_1 - A_2)^2 \tag{4.6}$$

$$A_3^2 = (x_2 - A_1)^2 + (y_2 - A_2)^2 \tag{4.7}$$

$$A_3^2 = (x_3 - A_1)^2 + (y_3 - A_2)^2, \tag{4.8}$$

and their solutions are:

$$A_1 = \frac{x_2^2 + y_2^2 - x_4^2 - y_4^2 + 2Dy_4 - 2Dy_2}{2(Cy_2 - Cy_4 - (x_4 - x_2)} \tag{4.9}$$

$$A_2 = D + CA_1 \tag{4.10}$$

$$A_3 = \sqrt{A_1^2 + A_2^2} \tag{4.11}$$

$$C = \frac{x_2 - x_3}{y_3 - y_2} \tag{4.12}$$

$$D = \frac{x_3^2 + y_3^2 - x_2^2 - y_2^2}{2(y_3 - y_2)}. \tag{4.13}$$

The fit procedure requires estimated initial parameters, so an average A_3 is determined in the procedure taking into account the three space points.

At this point, the space points with the initial parameters are taken in FIRSTCHECK and the first fitted points are calculated and the first χ^2 generated to determine whether an iteration process is necessary on the χ^2. That is, if the χ^2 is less than 10,000. Fitted space points are found by:

$$fity_i = A_2 + \sqrt{A_3^2 - (x_i - A_1)^2} \tag{4.14}$$

The data is now transferred to the circle fit (CIRFIT) which uses an iteration grid search method to minimize the χ^2 value by incrementing the parameters individually. This method is best used when the parameters of the function being used to fit are independent from each other. That means an optimization based on minimizing χ^2 for each individual parameter does not affect the fit. Large initial χ^2 fits of 10,000 and higher are not handed to the iteration process. They are labeled as non-primary tracks. Only two cases of data are being fitted: those that are four space points that represent a true track and those that have points on one or more layers of the SVT that have been traded for the actual point through a cone determination in search of a space point within the cone dimension on the next barrel. For actual tracks, when the fitted points are initially determined with the parameters calculated from CALC, the χ^2 values will be very close to one, if not below one. χ^2 is determined by summing the difference squared of fitted points to data points and dividing by the σ_i squared (σ_i is 100 μm: the wafer resolution times 4) (refer to equation 1.7). This is equivalent to a reduced χ^2, because the degrees of freedom of the fit is one (the number of data points subtracted from (the number of parameters+1) [7]. In the iteration, χ^2 is determined repeatedly with one parameter incremented by a delta value (Δ) in one direction and if it increases the increment is reversed and χ^2 is determined again to see if it has decreased. Once a decrease in χ^2 is found the iteration continues in that direction until the χ^2 increases again.

At this point, the routine calculates the value of the lowest χ^2 by finding the minimum from the last three points with a parabolic interpolation and determines the value of the parameter with the lowest χ^2 and the process continues for the next parameter until all parameters have been completed, or in graphical terms, until all parameter space has been searched for the lowest χ^2 value. The iteration method was taken from Bevingtons work in *Data Reduction and Error Analysis for the Physical Sciences* and he has presented the procedure of the grid search in steps:

1. One parameter A_J is incremented by a quantity Δ, where the magnitude of this quantity is specified and the sign is chosen such that χ^2 decreases.
2. The parameter A_J is repeatedly incremented by the same amount Δ until χ^2 starts to increase.
3. Assuming the variation of χ^2 near the minimum can be described in terms of a parabolic function of the parameter A_J, we can use the values of χ^2 for the last three values of A_J to determine the minimum of the parabola.
4. The minimum of the parabola is given by
$$A_{Jmin} = A_3 - \Delta * (((\chi_3^2 - \chi_2^2)/(\chi_3^2 - 2 * \chi_2^2 + \chi_1^2)) + 1/2) \tag{4.15}$$
5. χ^2 is minimized for each parameter in turn.
6. The above procedure is repeated until the last iteration yields a negligibly small decrease in χ^2[7].

This subroutine uses function subprograms FUN and FCHISQ to calculate the dependent variables and the χ^2. After finishing CIRFIT the fit is not complete because this procedure only describes the helix in the xy plane where the track is known to be a circle.

The third dimension to the helix is the linear characteristic in the circular plane called s in this case. Displacements in s are determined by

$$s_i = A_3 arcsin\left(\frac{\sqrt{x_i^2 + fity_i^2}}{2A_3}\right), \tag{4.16}$$

where i is the space point layer. Again, since this part of the helix is linear, the algorithm used is based on the least-squares method for a linear function and χ^2 is determined the same way as in the xy plane (SLINFIT). The total χ^2 results from the addition of the two fits in the xy plane and sz plane.

The next step in the program is to select all tracks characterized by their first space point that have the lowest χ^2 value. This is accomplished in SVT SELECT where the parameters, uncertainties, fitted space points, and χ^2's are stored in arrays for use later in SVT EFFIC.

4.4 Efficiency for Track Fit (SVT EFFIC)

The efficiency analysis after SVT FIT is called SVT EFFIC. Its primary purpose is to quantify an efficiency by comparing the array of the space point tracks iterated in the fit procedure to the actual GEANT tracks, input for SVT FILL. Tracks can be lost if the deviation between space points of a track does not fall within the cone restriction defined or the χ^2 of a ghost track is lower than the original GEANT track compared to in the fit iteration. The tracks are compared by a nested loop and then the fitted tracks are examined to store all χ^2 tracks greater than a value that extracts as many secondaries out of the track array as possible without also extracting many primaries. The size of this high χ^2 track array is dependent on χ^2 cut. These tracks with high χ^2 are put through a helix determination of the three space points excluding the origin to identify secondary tracks, those tracks having a vertex other than the primary vertex (DETER and LINDETER). A lower cut in χ^2 means more secondaries are determined, but also increases ghost secondaries (true primaries collected in the high χ^2 array). These determined three point tracks are than sent to SVT VERTEX to search for secondary vertices. All fitted tracks and their parameters are then transformed into usable TPC analysis shell parameters using structures through the subroutine TASDETER (Table 4.1).

Table 4.1: *TAS parameters*

Parameters	*Uncertainties*	*Description*
r_0, ϕ_0, z_0	Δr_0, $\Delta\phi_0$, Δz_0	Reference point of helix in cylindrical coordinates;
ψ	$\Delta\psi$	Azimuthal angle of momentum at first SVT point;
tanl	Δtanl	slope of linear fit at first point
invp	Δinvp	1/momentum at first point

4.5 SVT VERTEX: Determining Secondary Track Vertices

The SVT VERTEX routine takes two tracks of the resulting high χ^2 track array created in SVT EFFIC from the lowest χ^2 array selected in SVT FIT. Its purpose is to find two tracks that intersect from the array. Ideally, this determines two secondary tracks and their origin. Though, other ghost or virtual intersections can be present.

The subroutine sorts through the array using a nested loop. The first track is paired to each other track to check for a mutual intersection and then the loop moves on to the second track in search of an intersection. The search is performed in the y dimension of the tracks solving the equation below with a simple iterative process looking for the common y component in y_{v1} and y_{v2} which represents the y position of the vertex when they are equal.

$$y_{v1} = \sqrt{r_1^2 - (x_{v1} - x_{c1})^2} + y_{c1} \tag{4.17}$$

$$y_{v2} = \sqrt{r_2^2 - (x_{v2} - x_{c2})^2} + y_{c2} \tag{4.18}$$

r_1 and r_2 are the radii of the first and second tracks being compared. x_{v1} and x_{v2} are the vertex x position when they equal. x_{c1}, x_{c2}, y_{c1}, and y_{c2} are the corresponding center positions for the two helical tracks. The iteration continues in the direction where the difference in the y component of the two tracks $|\mathtt{y_{v1}} - \mathtt{y_{v2}}|$ is decreasing. If no intersection is found when $|\mathtt{y_{v1}} - \mathtt{y_{v2}}|$ increases after a decrease, the procedure ends.

If an intersection is found, the procedure continues to check if the xy intersection is a true intersection for three dimensions in the sz plane. The track is linear and an assumption is made that the track, when extrapolated, will traverse the $x = 0$ plane for a reference point which is used to find the z-intercept (z_o) in the sz line equation. Note that secondary tracks that do not truly intersect the $x = 0$ plane are lost, so a duplicate procedure with y = 0 plane could increase vertex search capabilities. Arc lengths are calculated for the s plane from x and y and a slope is found. The z_{v1} and z_{v2} are the same point if the lines intersect in this plane. The equations equated are:

$$z_{v1} = \theta_{v1} R_1 m_1 + z_{o1} \tag{4.19}$$

$$z_{v2} = \theta_{v2} R_2 m_2 + z_{o2} \tag{4.20}$$

The θ's are the angle in polar coordinates of the space points and the m's are the slopes in the sz plane.

Chapter 5

Features and Performance of the SVT Track Fitting Program

5.1 Introduction to the Capabilities and Results of the Fit Procedure on Selected Events

With FRITIOF and GEANT to simulate events and provide the detector geometry and tracking expected for STAR, SVT FIT (STRUGGLE) can be tested for performance on selected events. Due to the limitations of the computer software utilized and execution time, all events analyzed are bound to regions in η, but unrestricted in azimuthal angle ϕ, of the total SVT. The acceptance per event assuming the complete SVT is about 3000 charged particles and for the restricted events about 800 are within the region chosen. For the cases where the acceptance is around 800 tracks, the angle restrictions are θ_{min} = 1.1071 and θ_{max} = 2.0344 in radians and knowing the relationship between θ and η ,the pseudo-rapidity, as given earlier in equation 1.2, the η restriction is calculated to be η_{max} = 0.4813 and η_{min} = -0.4812. Note that the maximum pseudo-rapidity, as defined, corresponds to the minimum polar angle. This restriction provides a symmetric region in polar and azimuthal angle with respect to the beam axis. By not using the full SVT acceptance the density of charged tracks for this region is decreased by a slight percentage. This is because secondaries that would traverse this region with vertices outside the restriction of the event generator are prevented from doing so. Since secondaries consist of only about 10% of the total event and the percentage that would be given a velocity out of the region as defined above has been studied for three typical events and found to be about 6% of all secondaries (or less than 1% of the overall number of tracks). The effect is not substantial.

The quality of the fit for a track is defined by the χ^2 statistical parameter presented in equation 1.7. A typical χ^2 distribution is plotted in figures 5.3 and 5.4 for an event with the restricted region defined above. It should be noted that with $\sigma_y = 100\ \mu$m the majority of tracks have a χ^2 less than 400. (equivalent to a mean deviation for the 4 space points of 1000 μm). The χ^2 distribution of a similar event without MCS turned on during GEANT tracking is shown for comparison (figures 5.1 and 5.2). A breakdown of a typical event is described in the following sections along with a definition of the track efficiency and the fit procedure performance.

5.2 Optimization of the Fit Efficiency

The ability for the fit algorithm to retrieve and fit the correct tracks from the array of space points is dependent upon the SDD resolution and the amount of ghost tracks collected by the cone procedure. The detector resolution of a space point is expected to be 25μm absolute in all dimensions, but as the resolution increases efficiency will decrease, because more space points will be within the resolution of another, and thus indistinguishable.

The cone analysis, covered extensively in chapter 4, showed that an iterative in-

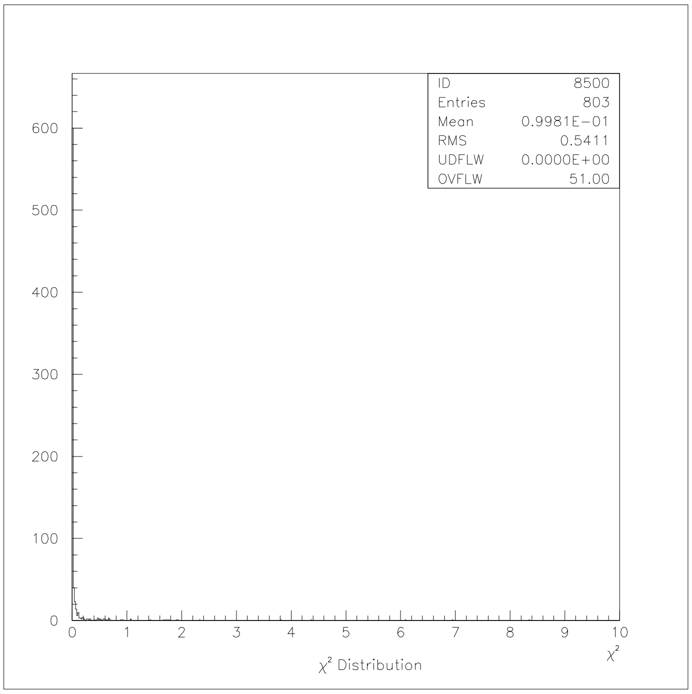

Figure 5.1: *The distribution of χ^2 for the fitted tracks of an event with no MCS and χ^2 defined as in chapter 1.*

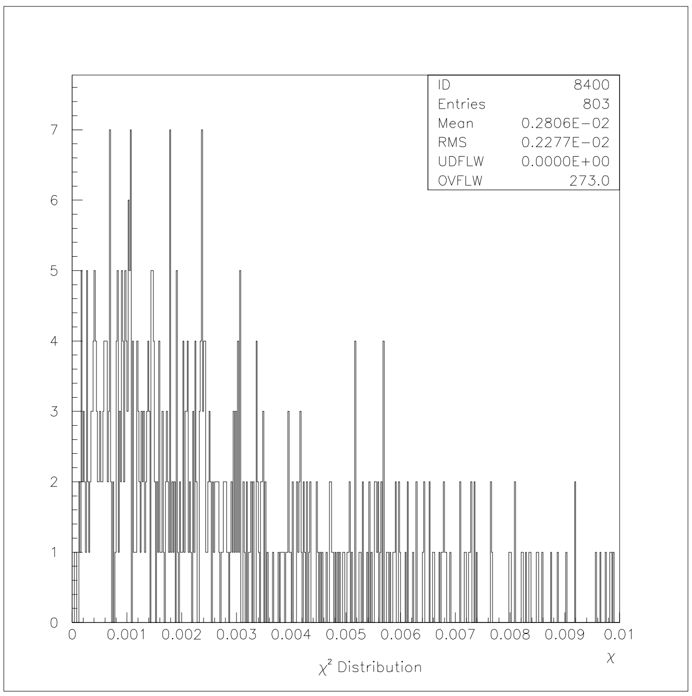

Figure 5.2: *The distribution of χ^2 for the fitted tracks near the minimum with no MCS χ^2 defined as in chapter 1.*

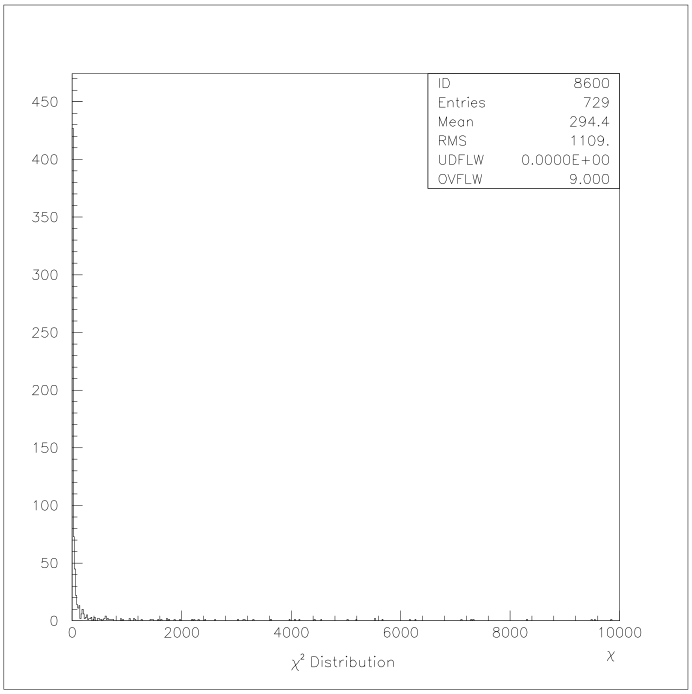

Figure 5.3: *The distribution of χ^2 for the fitted tracks with χ^2 as defined in chapter 1.*

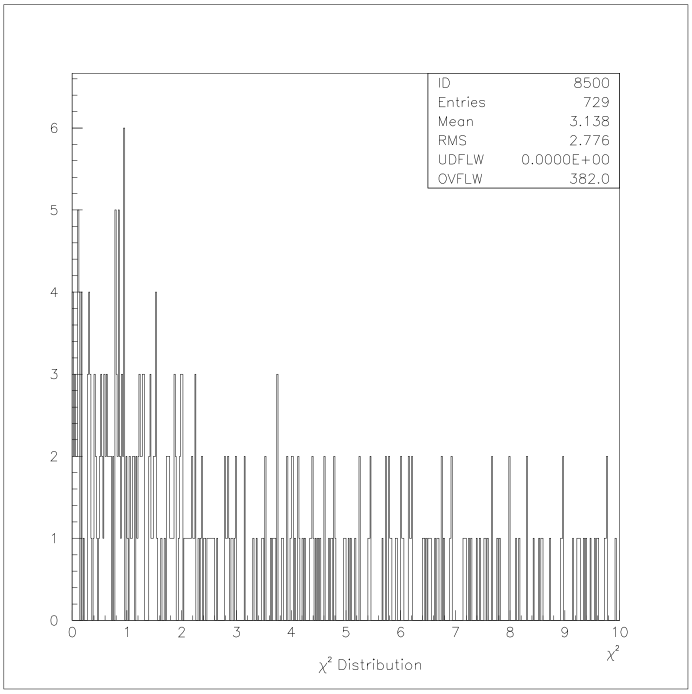

Figure 5.4: *The distribution of χ^2 for the fitted tracks near the minimum with χ^2 as defined in chapter 1.*

cremented cone and fit process to reduce the number of ghost tracks formed is the solution. A comparison plot of a fixed cone and fit procedure performed on an event and an incremented cone and fit process is in figure 5.5. The fit efficiency is defined as the ratio of the number of retrieved fitted original GEANT tracks to the number of original GEANT tracks with three space points (hits) of the restricted η event. The difference in the procedures is seen in the larger cone dimensions. Here, the fixed cone will take in many more ghost tracks than the incremented iterative process which removes prior fitted tracks from the array. Tracks that are most susceptible to replacement by ghost tracks are secondaries that project back away from the primary vertex and result in a high χ^2, but as figure 5.6 shows a larger percentage of primaries are also retrieved by incrementing the cone. Secondaries, as well as, primaries account for the higher efficiencies at large cones for the incremented cone that were being lost in the fixed cone method (see figures 5.6 and 5.7 for primary and secondary efficiencies), but the percentage of secondaries retrieved is twice as improved as the percentage of primaries. Note that the incremented cone procedure has another advantage at these larger cones in that it can continue to increment beyond the cone dimension in the plot in search of secondary tracks, while the fixed cone at larger cones will continue to produce more ghost tracks and burden the fit procedure with a huge input track array (see again figure 4.7 and 4.8).

It is important to realize that the fit efficiency defined is independent of the value of χ^2. This is done so secondaries can be retrieved with very high χ^2's which later can be taken out of the array, put into a helix track determination of three space points, and used in SVT VERTEX to search for secondary vertices. It is more correct to

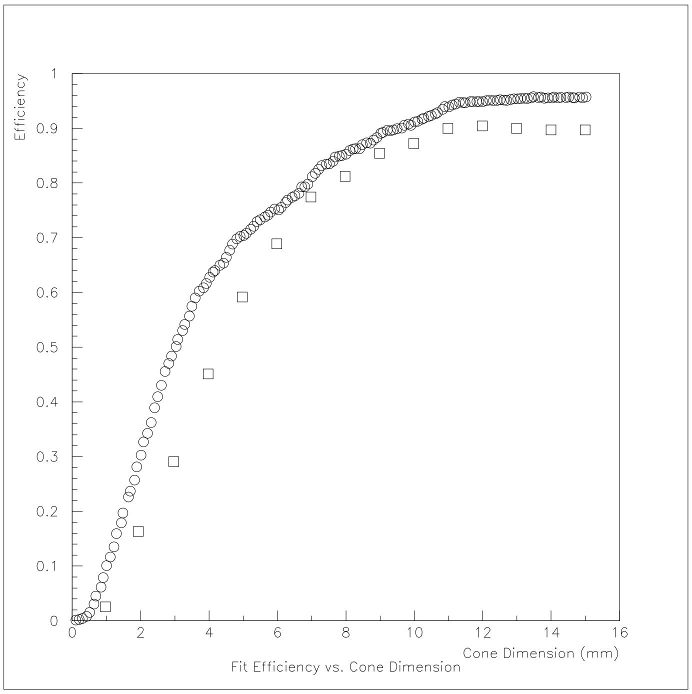

Figure 5.5: *The fit efficiency, as defined in the text, vs. the absolute cone dimension. The squares represent the fit efficiency with the cone dimension held constant for the fit of the event and the circles show the improvement of the efficiency when the cone is incremented and the tracks found at the cone increment are taken out of the iteration.*

call the secondary efficiency a track efficiency. The secondary track efficiency is based on the total number of secondary tracks originating inside the SVT($r < 5$ cm). For reference, secondaries originating after the first layer of the SVT to the beginning of the TPC ($r \approx 50$ cm) increase this number by about 60%.

5.2.1 Track Fitting Primaries

Tracks having an origin at the collision vertex are primaries. Primary tracks that traverse three layers of the SVT fulfill the requirements needed to fit a helical curve to the track. The minimum transverse momentum (p_t cut) for a track to leave the complete SVT is determined from the following derivation. From the second law of

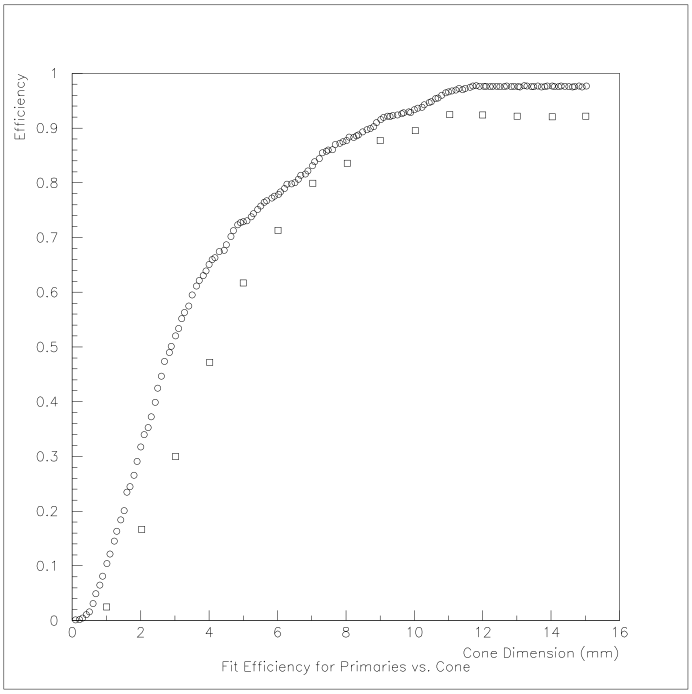

Fit Efficiency for Primaries vs. Cone

Figure 5.6: *The fit efficiency of the primaries of the same event shown in the earlier figure of the overall fit efficiency. The squares represent the fit efficiency with the cone dimension held constant and the circles show the efficiency when the cone is incremented.*

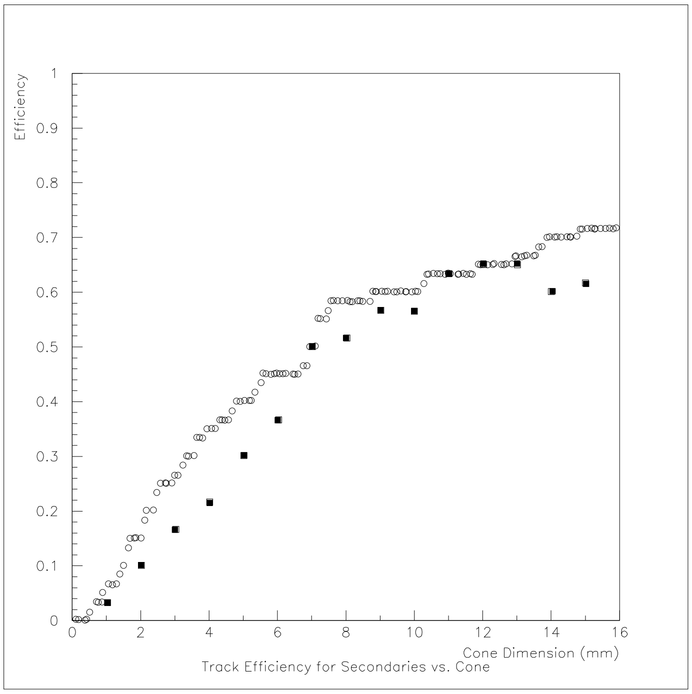

Track Efficiency for Secondaries vs. Cone

Figure 5.7: *The track efficiency of the secondaries of the same event shown earlier of the overall fit efficiency. The squares represent the fit efficiency with the cone dimension held constant and the circles show the efficiency when the cone is incremented.*

Newton assuming centripetal acceleration for circular motion,

$$F = ma = \frac{mv^2}{r}, \tag{5.1}$$

and Lorentz's equation of a charge particle moving in a magnetic field,

$$\vec{F} = q\vec{v} \times \vec{B} \tag{5.2}$$

or in magnitude,

$$F = qvBsin\theta \tag{5.3}$$

where $\theta = 90^o$. Thus, the relation between momentum and the radius of curvature is

$$rqB = p. \tag{5.4}$$

The radius of the helix in the xy plane is r and must be greater than half the maximum radius of the SVT for a charged particle to travel through all layers of the SVT. For Z = 1 charged particles, this minimum p_t is about 12 MeV/c. Tracks that do not leave three space points in three consecutive layers are not directly retrievable. Specifically, charged particles that do not traverse all layers have either a:

- $p_t < 12$ MeV/c
- track direction that traverses the side of the SVT
- decay into secondaries

If three layers are traversed for a particle with a primary vertex, the track can be retrieved and fitted. The p_t cut of the cone dimension used to collect primary tracks

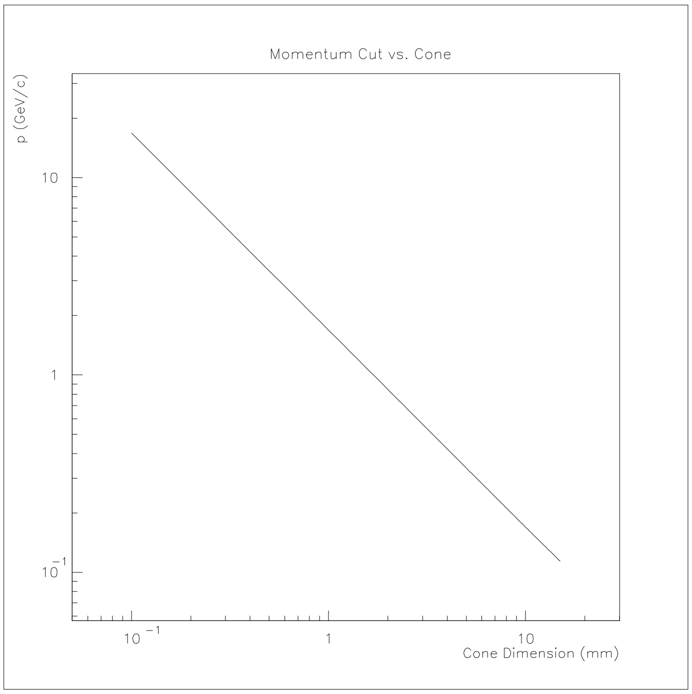

Figure 5.8: *The momentum cut defined by the cone dimension restriction, since momentum is related to the radius as shown in the text.*

is shown in the plot of figure 5.8. Tables 5.1 and 5.2 show a typical fit efficiency for an event with the restriction in η discussed. For comparison, a similar size event with the same restriction in η, but no MCS is presented in tables 5.4 and 5.5.

5.2.2 Track Determining Secondaries

The attempt to determine secondary tracks and their origin is part of the subroutines SVT EFFIC and SVT VERTEX as described in chapter 4. Since a secondary track in reality does not originate at the primary vertex, only three points are available to track its path. Secondaries that exist in the track array to the helix fit routine will fit with high χ^2 as compared to most primaries tracks, that is, if the secondary vertex is further away than the primary vertex resolution. These high χ^2 tracks as

Table 5.1: *Separating the overall efficiency into primary and secondary tracks for a particular track event.*

Part of Event	*Total*	*Primaries*	*Secondaries*
Number of Tracks in Event	751	695	56
Efficiency	0.9587	0.9755	0.75

Table 5.2: *Efficiency of fitting tracks by particle type of an event with a total particle count of 751 as in the analysis above.*

Particle Type	*Pions*	*Kaons*	*Protons*
Number of Particles	647	53	31
Efficiency	0.9567	0.9811	0.9677

Table 5.3: *The description of high χ^2 ($\chi^2 > 1225$) tracks in the 720 original GEANT tracks fitted and retrieved.*

Track Types	*Total*	*Primaries*	*Secondaries*
Number of Tracks	46	27	19

mentioned are taken out of the fitted track array. Tables 5.3 and 5.6 (without MCS) show the constituents of the high χ^2 array for a typical event (with χ^2 cut = 1225). Some primaries are collected in the high χ^2 array (60% of tracks with MCS and 10% without). Defining the total number of secondaries as those originating before the first layer, a simple calculation with secondary data given in the tables shows that around 70% are ghost primaries (secondaries with their $\chi^2 < \chi^2$ cut). The high χ^2 array of the fitted tracks are considered secondaries and are put through the three space point helix determination calculation. Note that secondaries can not be fitted and the χ^2 does not apply when the helix is determined. The results of secondary vertex finding will be discuss more in a later section.

Table 5.4: *Separating the overall efficiency into primary and secondary tracks for a particular track event with no MCS.*

Part of Event	*Total*	*Primaries*	*Secondaries*
Number of Tracks in Event	821	759	62
Efficiency	0.9817	1.0	0.7826

Table 5.5: *Efficiency of fitting tracks by particle type of an event with a total track event of 821 with no MCS, as in the analysis above.*

Particle Type	*Pions*	*Kaons*	*Protons*
Number of Particles	738	51	21
Efficiency	0.9810	1.0	0.9524

Table 5.6: *The description of high χ^2 ($\chi^2 > 1225$) tracks in the no MCS event where 806 original GEANT tracks were fitted and retrieved.*

Track Types	*Total*	*Primaries*	*Secondaries*
Number of Tracks	24	2	22

5.3 Origin Fit Resolution

The vertex resolution is determined from the distribution of the fitted origins of GEANT tracks with x as the independent variable and y and z as the dependents. Figures 5.9 and 5.10 show the primary vertex distribution for y and z dimensions with no MCS and superimposed with a dashed line is a similar statistic of events with MCS. The peak of the MCS vertex distribution is presented again with more statistics in figure 5.11 and 5.12 and have a full width half maximum of 400 μm for y and 100 μm for z, determined by the base of the fitted Gaussian curves(compare with CDR figures 4H-7,8, pages 4H-13,14) [1].

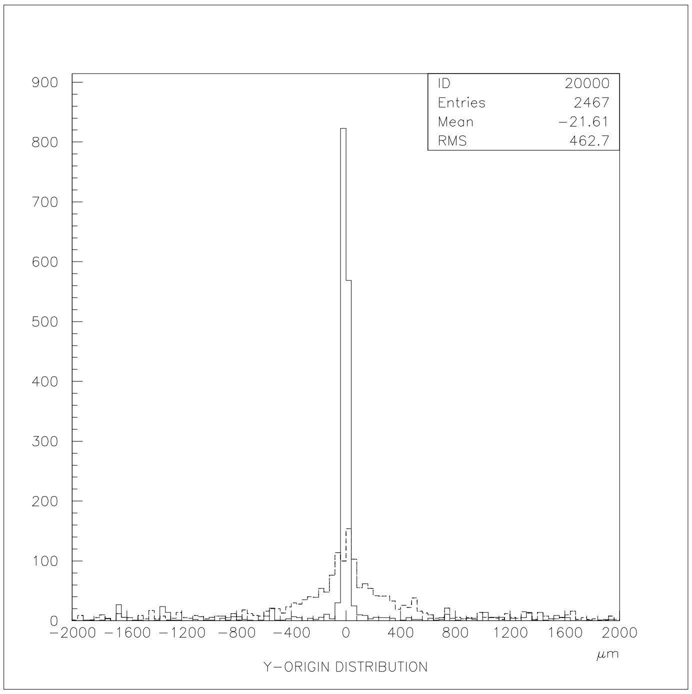

Figure 5.9: *The distribution of the projected y-component of the origin for the fitted tracks with and without multiple Coulomb scattering.*

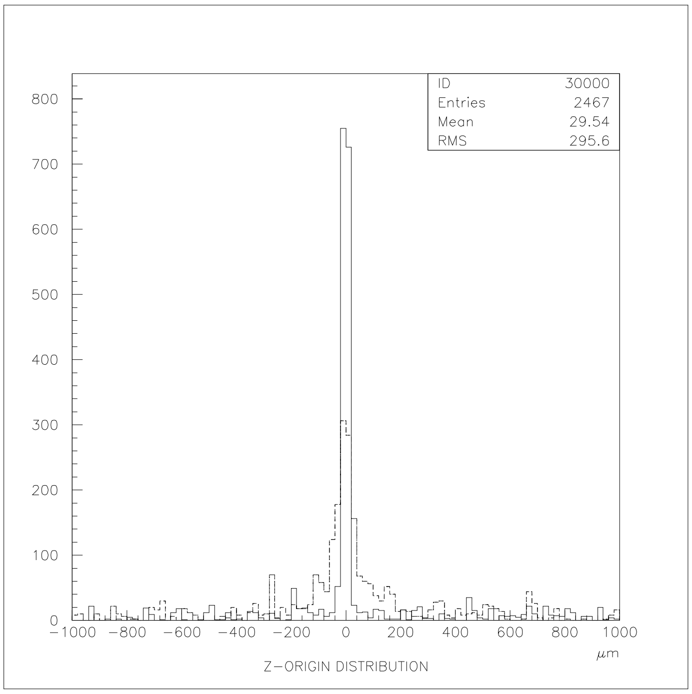

Figure 5.10: *The distribution of the projected z-component of the origin for the fitted tracks with and without multiple Coulomb scattering.*

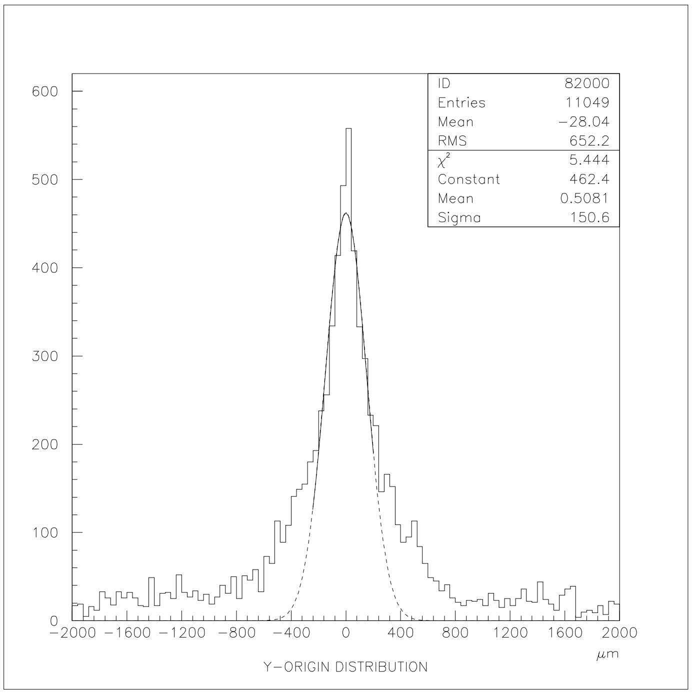

Figure 5.11: *The distribution of projected the y-component of the origin of ten fitted track events with a Gaussian fit applied.*

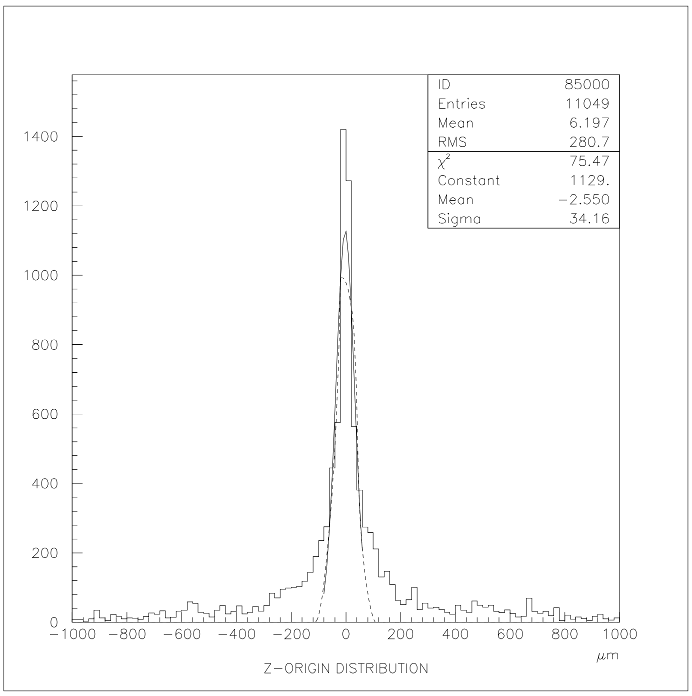

Figure 5.12: *The distribution of the projected z-component of the origin for ten fitted track events with a Gaussian fit applied.*

5.4 Momentum Resolution

5.4.1 Method of Analysis

The momentum resolution of the SVT depends strongly on the total momentum which is directly related to the radius of the helical track. This means the resolution of the radius dictates the resolution of the momentum. The radius is only determined as well as the fit is determined. The quality of fit is defined by the χ^2, so a resolution for a point on the helix can be extracted from χ^2 and applied to obtain the resolution of the radius which are not directly proportional. It should be realized that at some large radius defined by the χ^2 derived resolution the fit program will not distinguish the helical track from a straight line. This means in analytical terms that the uncertainty of this radius is infinity and every smaller radius with this χ^2 should be scaled to this maximum radius. Space point resolution from the χ^2 is determined by solving for the difference in the fitted to space point value of equation 1.7.

$$\sigma_{\chi^2} = \sqrt{(0.7)\chi^2\sigma_i^2} \tag{5.5}$$

σ_{χ^2} is the estimated fitted resolution in the space point at the third layer of the SVT (with radius about 15 cm)(see figure 5.13 for the geometry). The (0.7) factor is to allot 30% of the χ^2 to σ for the other two space points in the fit. With σ_{χ^2} of 100 μm at the third layer, determined from the space point resolution of the silicon wafer (SDD), the maximum helix radius detectable is about 112.5 m, or converting to momentum, the maximum momentum is 16.9 GeV/c. This means that at momenta higher than

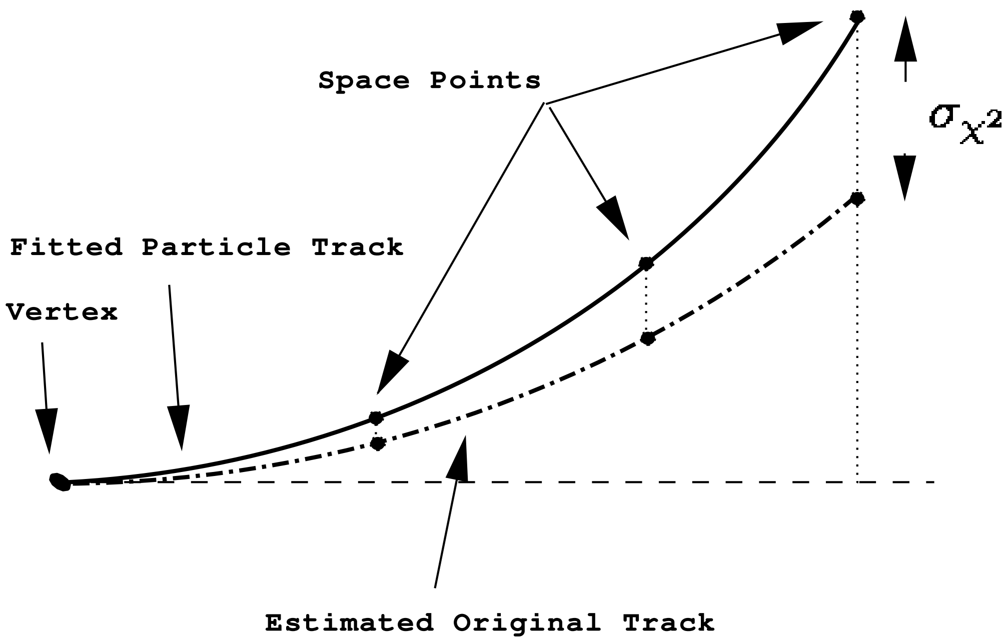

Figure 5.13: *The descriptive geometry of* σ_{χ^2}.

this cutoff, defined by the space point track resolution, the helix is approximated as a 3-dimensional line (refer to LINFIT subroutine), but few particles are in this range.

Knowing the fitted resolution σ_{χ^2} at the third layer, a radius of σ_{χ^2} difference in the third layer can be estimated. The difference between the radius of the fit and this estimated radius is an approximation of the radius resolution. The momentum is directly related to the radius, and therefore, so is their resolution. For a given particle type, certain momentum ranges are more common than others and the mean χ^2 ($\bar{\chi}^2$) varies between ranges. This will cause statistical effects in a plot of the momentum resolution, so to reduce this effect momentum bins are filled for 10 events and a $\bar{\chi}^2$ is determined for each bin. From the $\bar{\chi}^2$ of each bin, a momentum resolution is determined with an error bar, taken as the difference in the $\bar{\chi}^2$ determined momentum resolution at the point between two bins.

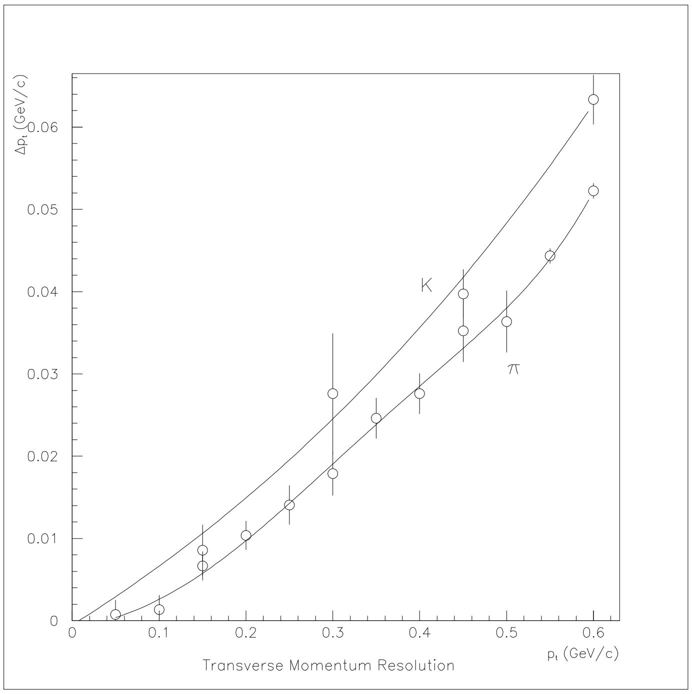

Figure 5.14: *The momentum resolution of fitted pion and kaon tracks from thirteen events with MCS determined by the* $\bar{\chi}^2$ *of selected momentum bins from .05 to .7 GeV/c.*

5.4.2 Results

This was done for π's and K's and plotted verses the transverse momentum (see figure 5.14). The curves compare qualitatively well with the expected momentum resolution plots in the June 1992 CDR for STAR (figure 4H-15, pages 4H-20) [1]. The results from the fit have a steeper increase near low momentum and in general are about 3% higher in resolution for both K's and π's.

5.5 Reconstruction of Decaying Particle Tracks

5.5.1 Vertex Reconstruction in General

The last routine SVT VERTEX determines secondary pairs by searching before the first layer for a secondary vertex between two tracks in the high χ^2 array which is a portion of the track array fitted and selected by the fit procedure. For these events, the portion of secondaries that have their vertex within the displacement window from the primary vertex of 400 to 50000 μm is about 40%. All secondaries are initially fitted as primaries, but 70% are stored as ghost primaries, because the high χ^2 cut chosen (those > 1225) determines this. Simply by decreasing the cut would transport more true secondaries into the high χ^2 array, but these would be accompanied by high resolution primaries which would than be ghost secondaries. This is a problem in determining secondary vertices. For the restricted events that are used in this study 20 to 30 tracks fall in the window. The procedure, with χ^2 cut = 1225, is able to retrieve about 60% (12 to 18 tracks) in the envelope and store them as high χ^2 tracks. Possible bad scenarios for detection of secondary vertices of two tracks in the high χ^2 array are:

- the two tracks are deflected by MCS causing the vertex position to change in space or disappear
- the secondaries project back to and within the resolution of the primary vertex
- a secondary particle track crosses within the resolution of another track stored in the high χ^2 not actually its secondary pair

These cases are found to be numerous and methods of over coming the percentage of secondaries lost to each are not complete.

Table 5.7: *Some particles likely to decay within the SVT geometry.*

	$c\tau$ (cm)	% in event	% decay before 1^{st} layer	decay in SVT	decay before TPC
K	371	4.8	1.3	4.0	13
Λ	7.9	1.0	47	85	99.8
Ξ	4.9	8.2×10^{-2}	64	95	100
Ω	2.5	4.1×10^{-6}	86	99.8	100
ϕ	resonance	3.3×10^{-3}	100	100	100

5.5.2 Relevant Particle Decays

Although the π ($c\tau$ = 7.8 m) decays, for the SVT geometry its $c\tau$ is too long. The list of decaying particles are in table 5.7. Reconstructing strange and anti-strange baryon decay scheme tracks are the most relevant for the physics of the SVT. In particular, the reconstruction of the following charged branches will be pursued (fraction of decay in parentheses).

- $\Lambda \rightarrow p\pi^-(64.1\%)$
- $\Xi^\pm \rightarrow \Lambda\pi^\pm$ (100.%) $\rightarrow p\pi^\pm\pi^\pm$ (64.1%)
- $\Omega^\pm \rightarrow \Lambda K^\pm$ (67.8%) $\rightarrow p\pi^\pm K^\pm$ (64.1%)

Notice, the reconstruction of multi-strange baryons requires the determination of tertiary vertices compared to the straight forward Λ reconstruction (detection of a single V-particle). The following describes a general approach to the problem of successive decays of a primary multi-strange baryon.

5.5.3 Ξ^- Reconstruction Scenario

With enough events, though, secondary vertices are determinable with the present software routine (Reference [27] explains successful Ξ^- searches at AGS with the TPC.).

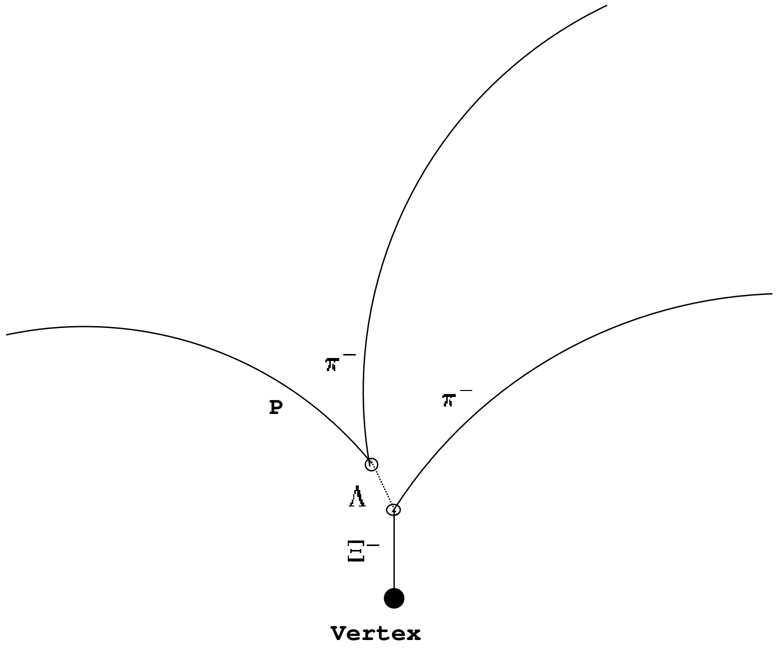

Figure 5.15: *The decay scheme of the Ξ^-.*

For example, the Ξ^- decay scheme shown in figure 5.15 should occur before the first layer. Since all resulting particles of this stage of the scheme are charged, they are detectable. The Λ which is uncharged connects the two vertices. The tertiary vertex of the proton and π^- could be found. With charged particles identified, by the TPC through dE/dx, and a mass reconstruction calculation knowing the momenta of the decay products from the relation with the radius of curvature, the Λ's momentum is obtained and thus, the slope of its track could be determined. It is a further study to see if p_id via dE/dx could be done in the SVT alone. The slope and the tertiary vertex point provide the information needed to reconstruct the linear Λ track back to an intersection with its decay partner, a π^-. This last search would require another routine that iterates an intersection search of a three-dimensional line and a helix.

Chapter 6

Conclusion and Improvements

6.1 Summary of Results

The proficiency of the track fitting software for SVT data space points in STAR is based upon knowing the original track array from GEANT. Information that is not available during the experiment. The track efficiency observed in these simulations will be used as an efficiency factor in the data analysis. All possible degradation factors (MCS, position and vertex resolution, various geometry options, etc.) can be taken into account. Because of the preliminary stage of the mechanical and electrical design for the SVT, the programs developed in this thesis are of general use and will be specifically applied in the future at any stage of the simulation, according to the latest design changes. Note, only the final design will provide the final efficiency factor.

Employing the presented simplified geometry, overall efficiency is around 95% of all tracks possessing three space points in three layers in the SVT. Primaries are track fitted to 98%. Secondaries are track retrieved at 75%. Events without MCS have efficiencies slightly higher than with MCS. MCS causes a difference of three orders magnitude higher in the χ^2 distribution shown in section 4.4, since the σ_y is held constant in the χ^2 definition (equation 1.7). This causes a simple shift in the χ^2

cutoff (distinction between primaries and secondaries), not in its pattern. Secondaries must be separated from primaries after fitting and determined without the origin. Note that secondaries with their vertex within the primary vertex resolution are lost and other secondaries with a vertex before the first layer cannot be fitted, but only helix determined without a vertex. The percentage of retrieved secondaries that are helix determined is highly dependent upon the chosen χ^2 cut. The case shown in chapter 5 with χ^2 cut $= 1225$ gives only about 30% secondaries to be determined. A lower cut would increase the secondaries determined, but increase ghost secondaries. Primary vertex and momentum resolutions are extracted to be slightly higher than preliminary results in the CDR of 1992. Secondary vertices are searched for by iterating in the y-dimension of two high χ^2 tracks. The success rate depends on controlling the haphazard scenarios defined in section 5.5.1.

6.2 Possible Improvements to the Software

In general, improvements of this software can be made in areas of time efficiency, secondary vertex tracing, and graphic display implementations. Time efficiency may require the program to be written at a lower level by utilizing structures or a more accommodating lower level language other than FORTRAN. Linearizing the parameter calculations would reduce some processing time. Hazards explained in chapter 5 need to be distinguished and avoided to improve secondary vertex determining. A better iteration method less dependent upon the cartesian coordinate system may be more successful. Approaches, based on 'neural network' pattern recognition are under investigation. A match to the TPC track would extend the number of space points on a track to a level where methods are applicable [28] [29]. The Software has been linked to graphic displays like PAW (Physics Analysis Workstation) HBOOK and PAW HIGZ (High level Interface to Graphics and Zebra), but the displays have not been developed beyond elementary steps. Graphic display would help in the area of secondary vertex reconstruction.

References

[1] *Conceptual Design Report for the Solenoidal Tracker At RHIC.* Berkeley, Ca.: The STAR Collaboration, (June 15, 1992).

[2] John Stachel, "Systematics of Global Observables in Relativistic Heavy Ion Collisions." talk presented at the VIIIth International Conference on Ultra-relativistic Nucleus-Nucleus Collisions. Menton, France, (1990).

[3] Z. Zhang, "Transverse Energy Measurements in Collisions of 14.6 GeV/c ^{28}Si and 11.4 GeV/c ^{197}Au Beams." Ph.D. thesis, Univ. of Pittsburgh, 1993.

[4] T.S. Tsai, *Rev. Mod. Phys.* 46, (1974) 815, as cited in *Physical Review D: Particles and Fields* New York: AIP, 1992.

[5] O.I. Dahl, private communication. as cited in *Physical Review D: Particles and Fields* New York: AIP, 1992.

[6] L. Brown, et al. ed. *Physical Review D: Particles and Fields* New York: AIP, 1992.

[7] Philip R. Bevington,*Data Reduction and Error Analysis for the Physical Sciences.* New York: McGraw-Hill Book Co., 1969.

[8] P.Rehak and E. Gatti, "State of the Art in Semiconductor Detectors." *Nuclear Instruments and Methods in Physics Research.* A289 (1990) pgs.: 410-417.

[9] T. Akesson et al., *Z. Phys.* C46 (1990) 361.

[10] H. Stroebele et al., *Z. Phys.* C38 (1989) 89.

[11] B. Jacak, *Nucl. Phys.* A525 (1991) 77c.

[12] E.V. Shuryak, *Nucl. Phys.* A525 (1991) 3c.

[13] L. van Hove, *Ann. Phys.* 192 (1989) 66.

[14] J. Bjorken, "A FAD Detector for SSC.", Colloquium. BNL, (May 1992).

[15] S. Pratt, Phys. Lett. B301 (1993) 153.

[16] J. Bjorken, Act. Phys. Pol. B23 (1992) 637.

[17] J. Rafelski, Nucl. Phys., A544 (1992) 279c.

[18] C.M. Ko, Plenary Session, QM93, to be published.

[19] D. Lissauer and E. Shuryak Phys. Lett. B253 (1991) 15.

[20] E.V. Shuryak, Phys. Rev. Lett., 68 (1992) 3270.

[21] R. Bellwied, STAR Note #108 (1993).

[22] R.Brun et al., *GEANT User Guide* CERN, (Sept 1987).

[23] *The LUND Monte Carlo Programs.* CERN, (Nov. 1, 1989).

[24] F. James, "Monte Carlo Theory and Practice." *Reports on Progress in Physics.* 43 (1980) 1145-1189.

[25] Torbjörn Sjöstrand. "The LUND Monte Carlo for Jet Fragmentation and e^+e^- Physics - JETSET VERSION 6.2." *Computer Physics Communications.* 39 (1986) 347-407.

[26] N.I. Chernov and G.A. Oskov. "Effective Algorithms for Circle Fitting." *Computer Physics Communications.* 33 (1984) 329-333.

[27] K. Zhao, "Observing Ξ^- in Heavy Ion Collisions at the AGS." RHIC School '93. BNL, (August 1993).

[28] C. Boymann, STAR Note #83 (1993).

[29] D. Liko, STAR Note August (1992).

[30] T Ferbel, ed. *Experimental Techniques in High-Energy Nuclear and Particle Physics.* New Jersey: World Scientific, 1991.

Abstract

A HELIX TRACK FITTING PROGRAM
FOR
THE SILICON VERTEX TRACKER (SVT)
IN
THE SOLENOIDAL TRACKER AT RHIC (STAR) EXPERIMENT

by

JOSEPH WILLIAM BIELECKI
December 1993

Adviser: Dr. Rene Bellwied
Major: Physics
Degree: Master of Science

The silicon vertex tracker (SVT) is a detector for low transverse momentum charged particles ranging from .05 to 1 GeV/c in the solenoidal tracker at RHIC experiment (STAR). STAR will be composed of colliding Au-Au beams with an azimuthal shaped detector system around the primary vertex. The major objectives of STAR are to investigate aspects of both soft physics like hadron production at transverse momenta below 1-2 GeV/c and hard physics processes in search of quark gluon plasma (QGP) signatures. The detector system will consist of the SVT (closest to the vertex), time projection chamber (TPC), magnetic field of 0.5 T, electromagnetic calorimeter (EMC), triggering detector system, and data acquisition (DAQ). The SVT constructed of three layers of silicon drift detectors (SDD) and with an acceptance of ± 1 in η will store three space points for each charged particle traversing all layers. With these space points and the vertex a fit can be performed to reconstruct the track. The tracks are helical due to the magnetic field. Event data and tracking are simulated on a Silicon Graphics Work Station using software packages FRITIOF and GEANT, respectively.

This thesis reviews the specific software developed for associating the space points into tracks, fitting the primaries, selecting original tracks out, and determining secondaries and their vertices. Efficiencies for track reconstruction is defined as the number of original tracks reconstructed over the number of original tracks. Overall efficiency is above 95%. Primary fitting is 98%. Secondary retrieving is near 75%, but methods for the reconstruction of secondary vertices is incomplete, because future development on controlling ghost intersections is pending. Origin and momentum resolution are investigated and found to be slightly higher than plots proposed in the conceptual design report. The difference in resolutions are largely caused by multiple Coulomb scattering.

Autobiographical Statement

Joseph William Bielecki

Personal:

Born - Detroit, Michigan, October 27, 1967
Married - Ivonne Valdez Santiago, May 29, 1993

Education:

Wayne State University (M.S.(Physics): 1993)
University of Michigan (B.S.E.(Aerospace): 1990)

Experience:

WSU Physics Teacher Assistant: Fundamental Physic Laboratory Teacher (1991-1993).
WSU DAPCEP Program Research Assignment: High School Prep Physic Laboratory Teacher (Fall 1992).
Chevrolet Pontiac Canada, General Motors Corporation, Summer Internship: Safety Restraint Systems Engineer (Summer 1989).

Publications and Presentations:

Aerospace System Design, University of Michigan. *Project EGRESS: Earthbound Guaranteed ReEntry from Space Station. The Design of an Assured Crew Recovery Vehicle for the Space Station.* NASA/USRA April 1990.

Status of the Testing and Implementation of the 93 W-car Rear Shell Mounted Retractor. presented at Safety Restraint Systems Group Meeting, CPC, August 25, 1989.

Scholarships:

WSU Physics Teaching Assistantship (1991-1993).
McDonnell Douglas Foundation Scholarship (1990).
John R. and Nora B. Everett Honorary Engineering Transfer Scholarship (1988).